Observational and model evidence for a prominent stratospheric influence on variability in tropospheric nitrous oxide

Cynthia D. Nevison[1], Qing Liang[2], Paul A. Newman[2], Britton B. Stephens[3], Geoff Dutton[4,5], Xin Lan[4,5], Roisin Commane[6], Yenny Gonzalez[7,8], Eric Kort[9]

[1]Institute for Arctic and Alpine Research, University of Colorado, Boulder, CO, USA
[2]NASA Goddard Space Flight Center, Greenbelt, MD, USA
[3]NSF National Center for Atmospheric Research, Boulder, CO, USA
[4]Global Monitoring Laboratory, NOAA Earth System Research Laboratory, Boulder, CO, USA
[5]Cooperative Institute for Research in Environmental Sciences (CIRES), University of Colorado, Boulder, CO, USA
[6]Department of Earth & Environmental Sciences, Lamont-Doherty Earth Observatory, Columbia University, Palisades, NY, USA
[7]CIMEL Electronique, Paris, 75011, France
[8]Izana Atmospheric Research Center, AEMET, Santa Cruz de Tenerife, 38001, Spain
[9]Department of Climate & Space Sciences & Engineering, University of Michigan, Ann Arbor, MI, USA

Correspondence to: Cynthia D. Nevison (cynthia.nevison@colorado.edu)

Abstract

The literature presents differing views on how variability in surface nitrous oxide (N_2O) is influenced by the stratosphere and whether forcings associated with the El Niño Southern Oscillation (ENSO) outweigh those influences. These issues are relevant to interpreting biogeochemical source signals in tropospheric N_2O and are investigated here using surface and aircraft-based atmospheric N_2O measurements and a chemistry-climate model with a stratospheric N_2O tracer. The model simulates well-defined seasonal cycles in tropospheric N_2O that are predominantly caused by the seasonal descent of N_2O-poor stratospheric air in polar regions with subsequent cross-tropopause transport and mixing. Similar cycles are identified in recently available data from global airborne surveys and aircraft-based monitoring. In the northern hemisphere, the annually-averaged surface N_2O atmospheric growth rate anomaly derived from long-term monitoring data is negatively correlated with winter (January-March) polar lower stratospheric temperature. This correlation is consistent with an influence from the Brewer Dobson circulation, which brings warm, N_2O-poor air from the middle and upper stratosphere into the lower stratosphere. In the southern hemisphere, the atmospheric growth rate anomaly is better correlated

to indices of ENSO and the stratospheric quasi-biennial oscillation (QBO). These hemispheric differences in the factors influencing the N_2O growth rate are consistent with known atmospheric dynamics and the complex interaction of the QBO with the Brewer Dobson circulation. More airborne surveys, which provide high-resolution N_2O data near the tropopause, would help refine our understanding of the stratospheric influence on the troposphere and enhance our ability to interpret surface N_2O sources.

1 Introduction

Nitrous oxide (N_2O) is an important ozone-depleting substance and long-lived greenhouse gas, with a global warming potential (GWP) of 265 relative to CO_2 over a 100 year time horizon (*WMO*, 2018). N_2O has an atmospheric lifetime of about 120 years and is destroyed slowly in the stratosphere by both photolysis and oxidation, with a fraction of the oxidation product yielding NO_x, a catalyst of stratospheric ozone destruction (*Crutzen,* 1970; *Prather et al.,* 2015). N_2O has abundant natural microbial sources in soil, freshwater and oceans, which account for the majority of global emissions, although anthropogenic sources are becoming increasingly important (*Tian et al.,* 2020; *Canadell et al*., 2021).

The atmospheric N_2O concentration has risen from about ~270 ppb preindustrially to 336 ppb by 2022 (*MacFarling-Meure et al*., 2006; *Lan et al.,* 2022). This rise has been attributed largely to Haber-Bosch industrial N fixation to produce agricultural fertilizer, which has increased the substrate available to nitrogen (N) cycling microbes (*Park et al.*, 2012). Recent evidence suggests that N_2O is increasing at an accelerating rate in the atmosphere, possibly due to a nonlinear response of microbes to increasing N inputs in intensively fertilized agricultural systems (*Thompson et al.*, 2019; *Liang et al.*, 2022).

High precision measurements of N_2O have revealed interannual variability in its atmospheric growth rate (AGR) and small-amplitude seasonal cycles in the range of 0.4 to 1 ppb (*Nevison et al*., 2004; 2007; 2011; *Jiang et al*., 2007; *Thompson et al.*, 2013). Spatial gradients in atmospheric N_2O are also small, e.g., the northern hemisphere (NH) minus southern hemisphere (SH) difference is approximately 1 ppb

(*Thompson et al.*, 2014b; *Liang et al.*, 2022). While larger spatial and seasonal signals in atmospheric N_2O have been observed at sites influenced by strong local agricultural or coastal upwelling sources (*Lueker et al.*, 2003; *Nevison et al.*, 2018; *Ganesan et al.*, 2020), at sites remote from local sources even variations of 0.2 ppb in estimated background N_2O levels can significantly affect the magnitude of N_2O emissions inferred from atmospheric inversions (*Nevison et al.*, 2018).

A few studies have inferred information about surface biogeochemical sources based on the observed seasonal cycle in atmospheric N_2O at remote monitoring sites. However, these studies have cautioned that the transport of N_2O-poor air from the stratosphere is a major cause of both seasonal and interannual variability in surface N_2O, which complicates the interpretation of surface emission signals (*Nevison et al.*, 2005; 2011; 2012; *Thompson et al.*, 2014b; *Ray et al.*, 2020; *Ruiz et al.*, 2021). Other studies have argued that El Niño Southern Oscillation (ENSO) cycles are the major driver of interannual variability in tropospheric N_2O (*Ishijima et al.*, 2009; *Thompson et al*., 2013; *Canadell et al*., 2021) or that ENSO-driven variability can obscure the influence of the stratosphere in some years (*Ruiz et al.*, 2021). ENSO refers to the periodic oscillation between warm (El Niño) and cold (La Niña) phases in the eastern tropical Pacific (ETP). During the El Niño phase, the warming and deepening of the thermocline is associated with reduced upwelling in the ETP and drought in South America, which can decrease oceanic and soil N_2O emissions, respectively (*McPhadden et al.*, 1998; *Ishijima et al.*, 2009; *Babbin et al.*, 2015).

Studies of the stratospheric influence on surface N_2O variability have differed with respect to the relative impact on the northern hemisphere (NH) and southern hemisphere (SH). *Ray et al.* (2020) found direct correlations between the stratospheric Quasi-Biennial Oscillation (QBO), lagged 8-12 months, and the observed surface N_2O AGR, but in the SH only. The QBO is a tropical, stratospheric, downward-propagating zonal wind variation with an average period of ~28 months that dominates the variability of tropical lower stratospheric meteorology (*Baldwin et al*., 2001; *Butchart*, 2014). *Ruiz et al.* (2021) found that, despite a clear correlation between the QBO and N_2O photochemical loss rates in the tropical middle stratosphere, variability in surface N_2O appeared to be governed by cross-tropopause

transport and mixing, rather than directly by the QBO. They showed evidence for a coherent influence of those dynamics on the surface N_2O seasonal cycle in the NH but not the SH.

Nevison et al. (2011) argued that cross-tropopause transport and mixing drives the N_2O seasonal minimum in both hemispheres, based on significant correlations between surface N_2O seasonal anomalies and stratospheric indices reflective of the Brewer-Dobson circulation (BDC). The BDC is a planetary-wave-driven, large-scale meridional circulation that transports ozone, greenhouse gases, and other constituents poleward and maintains the thermal structure of the stratosphere (*Butchart*, 2014; *Minganti et al.*, 2020). As part of this transport, the BDC brings warm, N_2O-poor air from the tropical middle and upper stratosphere into the polar lower stratosphere in the winter hemisphere (*Liang et al.*, 2008; 2009; *Nevison et al.*, 2011).

A better grasp of the controls on tropospheric N_2O variability has important implications for the interpretation of biogeochemical signals in N_2O data. If abiotic factors associated with the downward transport of N_2O-poor air from the stratosphere contribute significantly to variability, they must be disentangled from the data before inferring information about surface biogeochemistry and emissions. Understanding the influence of stratospheric variability on surface N_2O also may provide insight into anomalous changes in the AGR of CFC-11, which has a stratospheric sink similar to that of N_2O (*Ray et al.*, 2020; *Ruiz et al.*, 2021; *Lickley et al.*, 2021).

This paper explores the causes of variability in both the seasonal cycle and the AGR of tropospheric N_2O. It follows up on previous work by *Nevison et al.* (2011), who inferred a stratospheric influence in surface atmospheric N_2O data based entirely on correlations between interannual variations in stratospheric indices and detrended N_2O anomalies in months surrounding the seasonal N_2O minimum. In the meantime, altitude-latitude cross sections have become available from aircraft surveys that span a full seasonal cycle. In addition, advances in model development allow for explicit simulation of stratospheric N_2O tracers (*Ruiz et al.*, 2021; *Liang et al.*, 2022).

This study uses the NASA Goddard GEOS-5 Chemistry-Climate Model (GEOSCCM), which includes a tagged stratospheric N_2O tracer that is transported individually in the model and distinguished from tropospheric tracers of fresh surface emissions (*Liang et al.*, 2022). The study also examines atmospheric N_2O data measured by recent global airborne surveys spanning both hemispheres and collected by the National Oceanic Atmospheric Administration (NOAA) during routine aircraft monitoring in the NH. Finally, it performs an updated correlation analysis of surface N_2O anomalies from ground-based NOAA sites against ENSO and QBO indices as well as polar lower stratospheric temperature (PLST), which reflects the influence of the BDC.

The paper is organized as follows: Section 2 describes the data and methods used. Section 3 presents the results, beginning in Section 3.1 with an examination of climatological mean seasonal cycles and latitude-altitude cross sections of N_2O from GEOSCCM and aircraft data. Section 3.2 examines correlations between variability in the N_2O AGR from NOAA long-term surface monitoring data, PLST, and indices of QBO and ENSO, with the premise that significant correlations offer evidence of causation. Section 3.3 examines correlations between PLST and variability in monthly N_2O anomalies near the month of seasonal minimum. Sections 3.2 and 3.3 include parallel correlation analyses of variabililty in GEOSCCM N_2O sampled at NOAA surface sites and GEOSCCM-based QBO and PLST indices. Section 4 interprets and discusses the results. Section 5 finishes with a summary and conclusion.

2 Methods

2.1 GEOSCCM with tagged stratospheric tracers

GEOSCCM was used to simulate atmospheric N_2O with geographically resolved surface emissions from soil, ocean and anthropogenic sources, and full stratospheric chemistry with stratospheric N_2O destruction due to photolysis and $O(^1D)$ oxidation (*Nielsen et al.,* 2017; *Liang et al.*, 2022). GEOSCCM has been evaluated extensively in multi-model assessments and shown to represent well the mean atmospheric circulation, the interhemispheric exchange rate, the mean age of air in the tropical and polar stratosphere, and the mean atmospheric lifetime of N_2O (*Liang et al.*, 2022 and references

therein). For the current study, GEOSCCM was run at 1°x1° resolution with 72 vertical layers from the surface to 0.01 hPa. In addition to the standard total N_2O tracer, four additional N_2O tracers were included to track: 1) aged air from the stratosphere ($N2O_{ST}$), and 2) soil, 3) ocean, and 4) anthropogenic sources freshly emitted in the troposphere. Following the approach of *Liang et al.* (2008), the tropospheric tracers become the stratospheric tracer, $N2O_{ST}$, when they are transported across the tropopause, and retain that identity even when $N2O_{ST}$ re-enters the troposphere, thereby providing a model estimate of the stratospheric influence on tropospheric N_2O.

The full GEOSCCM simulation spanned 1980-2019, but this study focuses on the final 20 years from 2000-2019 for the correlation analysis between model surface N_2O anomalies and QBO and PLST. As described in detail in *Liang et al.* (2022), the GEOSCCM N_2O lifetime decreased slightly after 2000 (to 116 ± 2 yr in the 2010s down from 119 ± 2 yr in the 1990s) and model emissions were optimized to account for the observed change in the atmospheric N_2O growth rate. GEOSCCM temperature and QBO do not necessarily correspond to observations since both are internally generated by the GEOS general circulation model, which is free running rather than forced by a reanalysis meteorology. However, they were computed in the same way as the observed QBO and PLST indices, as described below in Section 2.4.1 and 2.4.2, respectively. The GEOSCCM N_2O fields were saved as monthly means and were detrended and converted to anomalies by subtracting a deseasonalized fit to the model time series sampled at Mauna Loa.

2.2 N_2O Data

2.2.1 Surface N_2O from NOAA long-term monitoring sites

Surface atmospheric N_2O data were obtained from the NOAA Global Monitoring Laboratory (GML) for comparison to GEOSCCM output. NOAA has two programs that measure N_2O, Halocarbons and other Atmospheric Trace Species (HATS) (*Thompson et al.*, 2004) and the Carbon Cycle Greenhouse Gases group (CCGG) (*Lan et al.*, 2022). HATS provides *in situ* data measured every ~ 60 minutes using the Chromatograph for Atmospheric Trace Species (CATS) instruments at 5 baseline sites (Barrow, Alaska; Niwot Ridge, Colorado; Mauna Loa, Hawaii; Cape Grim, Tasmania; and South Pole,

Antarctica). CCGG maintains a flask-air sampling network at ~55 widely distributed surface sampling sites, in which duplicate samples are collected about weekly and shipped to Boulder, Colorado for analysis by gas chromatography (GC) with electron capture detection and by a Tunable Infrared Laser Direct Absorption Spectroscopy (TILDAS) after August, 2019. The instruments are calibrated with a suite of standards on the WMO X2006A scale maintained by NOAA GML (*Hall et al.*, 2007). Uncertainties of the measurements (68% confidence interval) range from 0.26 to 0.43 ppb with GC-ECD and 0.16 ppb with TILDAS. The mean uncertainties in CATS GC data are 0.2 to 1.2 ppb (68% confidence interval) over most of the 2000s, with an increase in recent years as the instruments approach their lifetime.

This study used the NOAA combined HATS/CCGG N_2O product from 1998-2020, which is based on monthly medians from the CATS *in situ* program (at 5 sites) and monthly means from the CCGG flask program (at 13 background sites) (https://doi.org/10.15138/GMZ7-2Q16; *Hall et al.*, 2007). The combined monthly data are first aggregated at the measurement program level for each sampling location. If both HATS and CCGG measure at a location, a weighted mean is calculated based on the programs' monthly uncertainties. All of the NOAA sites considered in this study, including Alert, Canada; Summit, Greenland; Mace Head, Ireland; Cape Matatula, Samoa; Palmer Station, Antarctica and the HATS baseline sites listed above, are long-standing remote sites situated away from strong local anthropogenic sources. In addition to these individual sites, global, NH and SH means are estimated from the latitude-binned and mass-weighted means of the combined monthly means for 12 background sites (*Hall et al.*, 2011).

2.2.2 NOAA Empirical Background for atmospheric N_2O

The NOAA empirical background is a 4-dimensional (4-D) field, constructed from NOAA surface and aircraft N_2O data, which is used in North American regional inversions to represent the background concentration of atmospheric N_2O prior to the influence of continental surface fluxes (*Nevison et al.*, 2018). The 4-D field is defined daily over North America from 500-7500 m every 1000 m, from 170°-50°W every 10° longitude, and from 20-70°N every 5° latitude (or, prior to 2017, from 20-80°N every

10° latitude). To construct the field, NOAA data are categorized as marine boundary layer, free troposphere or continental boundary layer, depending on the location of each sample. These three categories are treated individually as follows: For the marine boundary layer, time- and latitude-dependent reference surfaces are computed separately for the Pacific and Atlantic (*Masarie and Tans*, 1995, updated as described in *Lan et al.*, 2023). For the free-troposphere, reference surfaces are created using a similar approach, with an additional "domain-filling" step informed by backward and forward trajectories for each aircraft sample collected above 3000 m AGL. For the continental boundary layer, N_2O data are detrended by subtracting the latitude and time dependent marine boundary layer reference values, where the transition from Pacific to Atlantic is represented by linear interpolation as a function of longitude across the continent. Then, a multi-year mean seasonal cycle is computed as a function of latitude, longitude, and day of year following *Hammerling et al.* (2012). For this study, a deseasonalized fit to the NOAA time series at Mauna Loa was used to detrend and remove the mean value (centered in the mid troposphere) of the empirical background data, thus allowing them to be collapsed into a single climatological year and presented as anomalies. The time period selected for the climatology was January 1, 2009-December 31, 2013, which roughly overlaps with the HIPPO airborne surveys described below, over a period when atmospheric N_2O was increasing by about 0.9 ppb/yr.

2.2.3 N_2O data from global airborne surveys

Atmospheric N_2O measurements were made *in situ* with the Harvard/Aerodyne Quantum Cascade Laser Spectrometer (QCLS) on three different aircraft campaigns designed to study the atmospheric profiles of greenhouse and related gases (*Wofsy et al.*, 2011; *Stephens et al.*, 2018). QCLS N_2O data are retrieved at 1-Hz with 1s precision of 0.09 ppb and reproducibility with respect to the WMO N_2O scale of 0.2 ppb (*Kort et al., 2011; Santoni et al., 2014*) on the NOAA-2006 scale (*Hall et al.*, 2007). The first of the these campaigns, the HIAPER Pole to Pole Observations (HIPPO) project, consisted of 5 roughly month-long sets of flights centered over the central Pacific Ocean extending from the surface to the upper troposphere/lower stratosphere and nearly pole to pole (*Wofsy et al.*, 2011). These flights were timed between January 2009 and November 2011 to create a climatological seasonal cycle. The second campaign (ORCAS), took place in January-February 2016 and focused on the Southern Ocean

south of ~35°S (*Stephens et al*., 2018). Most recently, the Atmospheric Tomography Mission (ATom) campaign extended nearly pole to pole over both the Pacific and Atlantic Oceans. ATom consisted of 4 deployments over 3 years, with each deployment approximately 1 month long (*Thompson et al.*, 2022). QCLS N_2O was measured during the second through fourth ATom deployments in January/February 2017, September/October, 2017 and April/May 2018, respectively, but N_2O measurements are not available from the first ATom deployment in July/August 2016 due to technical problems (*Gonzalez et al.*, 2021). For all figures presented below using QCLS N_2O, the flight track data were interpolated onto a 5 degree latitude by 50 hPa grid using the akima package in R (Akima, 1978). In addition, a deseasonalized fit to the NOAA time series at Mauna Loa was subtracted from all data, allowing them to be collapsed into a climatological year and expressed as anomalies**.**

2.3 Correlation analysis for surface N_2O

2.3.1 Interannual variability in the atmospheric growth rate

Interannual variability in the atmospheric growth rate of N_2O in the NOAA surface NH, SH and global time series was calculated by first removing the seasonal cycle from the monthly mean time series by computing a 12-month running average,

$$X_i = (C_{i-6} + 2\sum_{k=i-5}^{i+5} C_k + C_{i+6})/24, \quad (1)$$

where *C* is the original monthly mean time series and *X* is the deseasonalized time series. The slope of the deseasonalized time series then was computed as a central difference,

$$S_i = 12\ \frac{x_{i+1}-x_{i-1}}{2}, \quad (2)$$

where S is the centrally differenced slope and the scalar 12 converts *S* from units of ppb/month to ppb/yr. To account for the increasing growth rate of atmospheric N_2O, the absolute slopes *S* were converted to atmospheric growth rate anomalies by removing an optimal (increasing) linear fit determined by recursive least squares regression.

2.3.2 Interannual variability in the magnitude of the seasonal N_2O minimum

To calculate interannual anomalies in the magnitude of the seasonal minimum, the raw monthly mean N_2O data were detrended with a 3rd-order polynomial, after which a climatological seasonal cycle was constructed by taking the average of the detrended data for all Januaries, Februaries, etc. This climatological annual cycle was subtracted from the original raw data to produce a deseasonalized (but not detrended) time series. A running 12-month annual mean of this curve was then computed as in Equation 1, but where *C* is now the deseasonalized time series rather than the original monthly mean time series. This analysis focused on mid and high latitude sites in the NOAA dataset. At stations with gaps in the monthly data, the original 3rd order polynomial fit was used as a placeholder in the running mean. The running mean was subtracted from the deseasonalized curve to remove the secular trend and other low frequency variability, thus isolating the residual high frequency anomalies.

2.4 Proxies and indices for the correlation analysis

The computation of N_2O AGR anomalies from Section 2.3.1 created a set of monthly-resolved time series for the SH, NH and global means. These were plotted against various proxies and indices for both stratospheric influences and ENSO. In addition, the high frequency residuals from Section 2.3.2 at various mid and high latitude sites were sorted by month and selected months were plotted against the polar lower stratospheric temperature (PLST) BDC proxy described below.

2.4.1 Polar lower stratospheric temperature (PLST) as proxy for the Brewer Dobson circulation

Mean polar (60°-90°) lower stratospheric temperature at 100 hPa in January-March (winter) in the NH and September-November (spring) in the SH was computed from the Modern-Era Retrospective Analysis for Research Applications, Version 2 (MERRA-2) reanalyses (*Gelaro et al.,* 2017). PLST reflects the cumulative effect of fall/winter stratospheric downwelling due to the BDC (Holton, 2004). The mean PLST in each hemisphere was treated as a proxy for the integrated strength of the BDC, which brings warm N_2O-poor air from the middle to upper tropical stratosphere into the polar winter lower stratosphere, with warmer PLST corresponding to stronger downwelling (*Nevison et al.*, 2007; 2011). Winter months (January-March) were averaged in the NH and spring months (September-November) in the SH to account for the later seasonal breakup of the Antarctic polar vortex compared

to the Arctic polar vortex (*Nevison et al.*, 2011). For the monthly analysis, the PLST proxy was regressed against the monthly N_2O anomaly in each of the subsequent months leading up to and encompassing the seasonal minimum in tropospheric N_2O, which occurs in summer in the NH and autumn in the SH. For the AGR analysis, the mean N_2O AGR anomaly was averaged over 12 months (considering a range of start/end months) for regression against PLST.

2.4.2 Quasi-Biennial Oscillation (QBO)

The QBO was quantified using monthly mean stratospheric zonal wind values in m/s derived from twice daily balloon radiosondes conducted by the Meteorological Service Singapore Upper Air Observatory at a station located at 1.34°N, 103.89°E (https://acd-ext.gsfc.nasa.gov/Data_services/met/qbo/QBO_Singapore_Uvals_GSFC.txt). A positive QBO indicates westerly winds and a negative QBO indicates easterly winds. A range of altitudes from 10 mb to 100 mb was considered. Since the QBO index is a monthly mean time series, it can be compared directly to the monthly mean N_2O AGR time series. However, delays are expected between the QBO and its influence on tropospheric N_2O (*Strahan et al.*, 2015; *Ray et al.*, 2020). Therefore, a range of lag times was considered spanning 6-24 months when correlating with the N_2O AGR anomalies to identify the optimal QBO altitude and lag in each hemisphere.

2.4.3 ENSO

ENSO cycles were defined using the Niño 3.4 index, which is based on sea surface temperature anomalies from 5°S to 5°N and 170° to 120°W. The Niño 3.4 index defines an El Niño event as a temperature anomaly of > 0.4 degrees C and a La Niña event as a temperature anomaly of < -0.4°C. Monthly Niño 3.4 indices were obtained from https://www.cpc.ncep.noaa.gov/data/indices/sstoi.indices. Like the QBO index, Niño 3.4 is a monthly time series that can be compared directly to the monthly mean N_2O AGR time series. In the analysis presented here, a range of lag times in the Niño 3.4 index was considered spanning 0-12 months to identify the optimal lag in each hemisphere.

2.5 GEOSCCM correlation analysis

Equations 1 and 2 were applied to GEOSCCM N_2O output sampled at the coordinates of NOAA monitoring sites to create modeled N_2O AGR time series and monthly anomalies, using both total N_2O and N_2O_{ST}. Similarly, mean winter and spring PLST at 100 hPa was calculated for GEOSCCSM output in the NH and SH, respectively, as described in Section 2.4.1, for each model year from 2000-2019. Finally, a GEOSCCM monthly QBO index was calculated at a range of altitudes from 10 mb to 100 mb by averaging the model zonal wind component in m/s between 5°S and 5°N over each of the 240 months from 2000-2019. A correlation analysis was performed using the GEOSCCM N_2O AGR and monthly anomaly time series regressed against GEOSCCM PLST and QBO, similar to that described for the observed quantities in Sections 2.3-2.4. The ENSO correlation analysis was not applied to GEOSCCM output because the model did not attempt to reproduce the impact of ENSO on surface flux variability (*Liang et al.*, 2022).

3. Results

3.1 Stratospheric influence on tropospheric N_2O in model and aircraft data

Figure 1 shows that the GEOSCCM N_2O mean seasonal cycle at surface sites is dominated by stratospheric air depleted in N_2O that is transported to the surface, rather than by the influence of surface sources. However, the surface emissions tend to pull the total N_2O seasonal minimum about 1 month earlier than the $N2O_{ST}$ minimum at most sites. Figure 1 also shows that GEOSCCM captures the mean observed seasonal cycle in N_2O relatively well at sites in the SH but overestimates the amplitude of the cycle at sites in the NH, with a ~1-2 month delay in phasing relative to observations.

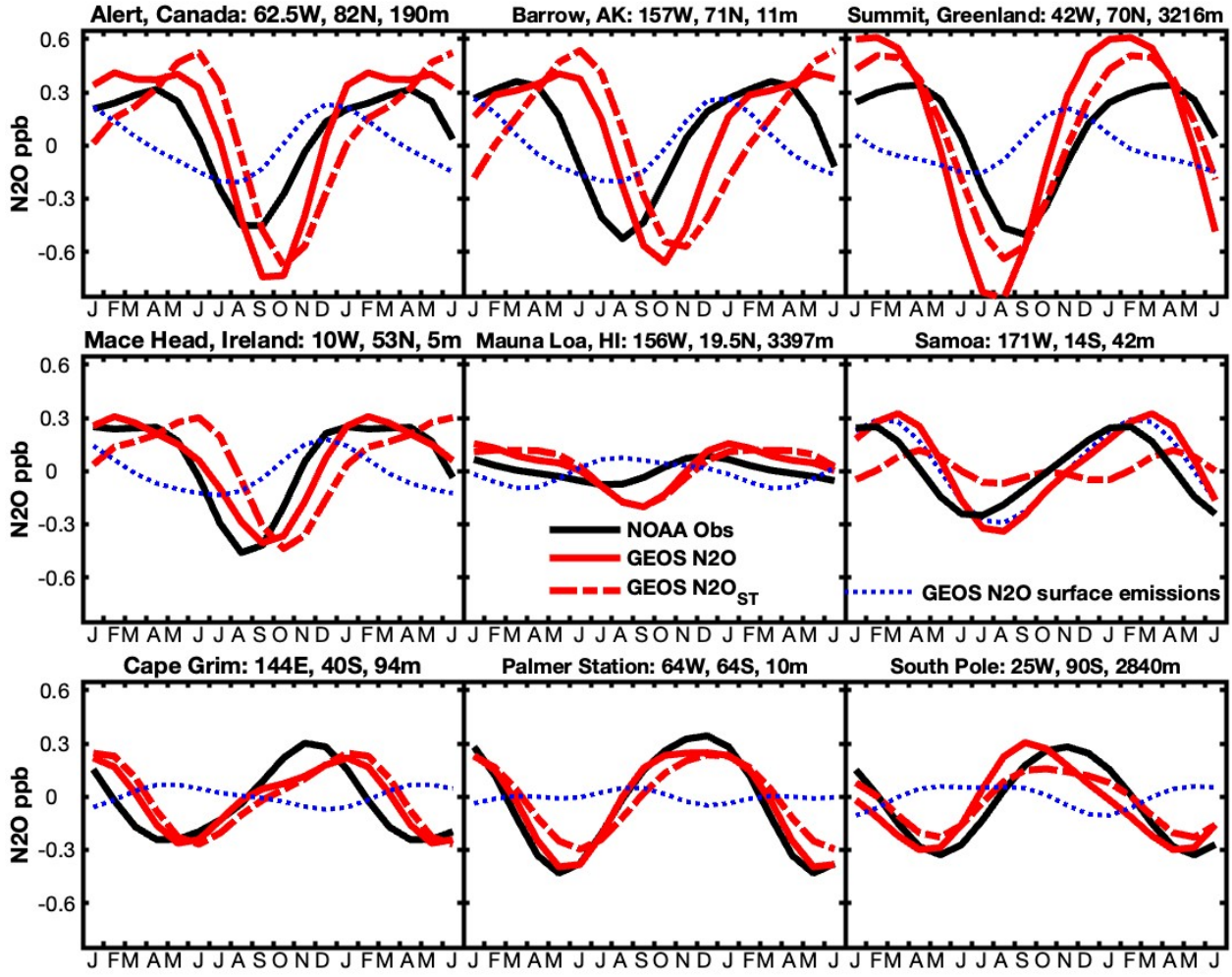

Figure 1: Detrended seasonal cycles in atmospheric N_2O modeled by GEOSCCM and compared to NOAA surface station data at 9 surface sites. Top row from left to right: Alert (Canada), Barrow (Alaska), Summit (Greenland); middle row from left to right: Mace Head (Ireland), Mauna Loa (Hawaii), Cape Matatula (Samoa); bottom row from left to right: Cape Grim (Tasmania), Palmer Station (Antarctica), South Pole (Antarctica). The black heavy line is observed N_2O from NOAA. For GEOSCCM, the total N_2O from all forcings is in red and the stratospheric tracer N_2O_{ST} is in dashed red. The dotted blue line is N_2O due to fresh surface emissions, representing the combined net influence of the natural soil, ocean, and anthropogenic atmospheric tracers.

Figure 2 provides a two-dimensional view, using zonally-averaged altitude-month contour plots at middle and high latitudes in both hemispheres, of how the signal of stratospheric air depleted in N_2O is transmitted to the surface in GEOSCCM. This N_2O-poor air accumulates during winter (starting in ~December in the NH and ~July in the SH) in the polar stratosphere, descends vertically and crosses into the troposphere in spring (March-April) in the NH and early summer (January-February) in the SH.

The SH latitude panels in Figure 2 are plotted with a 6-month shift to help visualize the later seasonal phasing of the stratospheric influence in the SH relative to the NH. After crossing into the troposphere, the N_2O-poor air continues to move downward, and also mixes equatorward, from approximately January to May at SH mid-to-high latitudes and April to October at NH mid-to-high latitudes. Due to lags in downward propagation and mixing, the modeled surface minimum in the lower troposphere does not occur until late summer to early autumn in both hemispheres (Figures 1 and 2). Supplementary Figure S1 shows a 3-dimensional view of this process in a series of 12 monthly altitude by latitude plots.

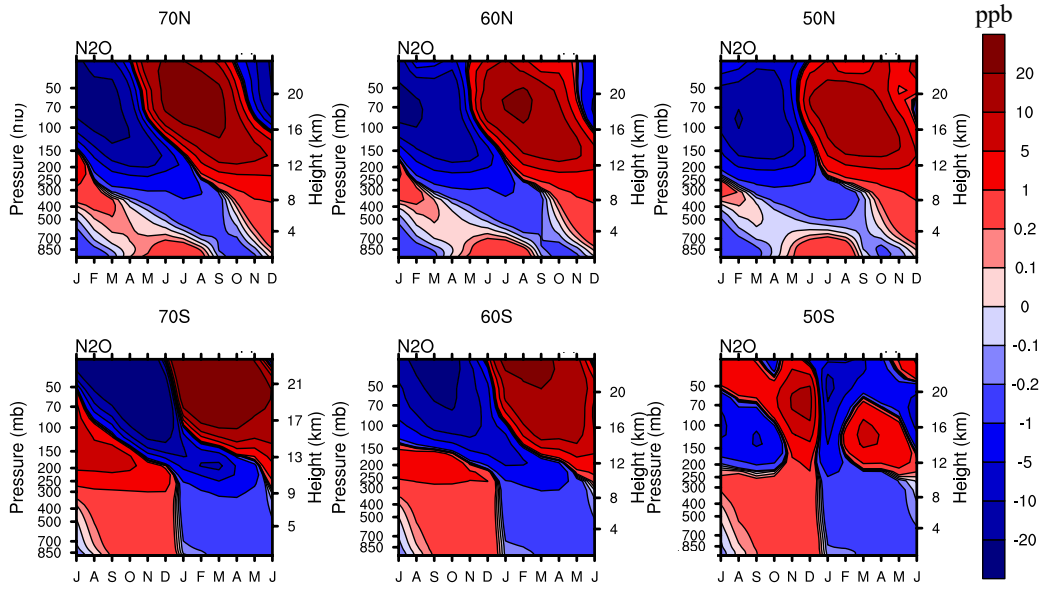

Figure 2: GEOSCCM N_2O anomalies in ppb as a function of month and altitude over a mean seasonal cycle, plotted from the surface to 30 hPa in the NH (top row) and SH (bottom row). From left to right: 10° latitude bins centered at 70°, 60° and 50°. Monthly anomalies are computed by subtracting the annual mean value at each pressure level.

Figure 3 shows that the NOAA N_2O empirical background, when organized as a series of zonally-averaged altitude-month contour plots at NH latitudes, has features similar to those simulated by GEOSCCM. Both model and observations show a signal of N_2O depletion beginning in early spring in the upper troposphere that propagates down to the surface. In both model and observations, the signal is strongest at high latitudes and weakens substantially moving equatorward. However, the NOAA data suggest a faster, more direct downward propagation of the stratospheric signal, which arrives at the

surface in August-September, compared to September-October in GEOSCCM. As a result, the phasing of the GEOSCCM surface minimum is delayed ~1-2 months relative to the NOAA empirical background, consistent with the comparison to NOAA surface monitoring data in Figure 1.

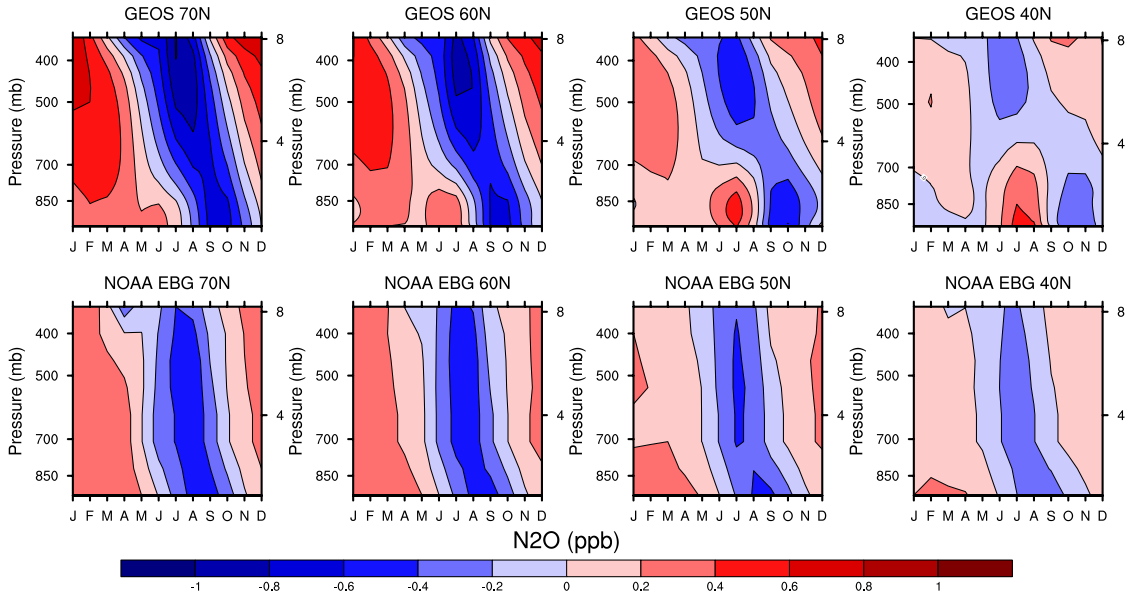

Figure 3: N_2O anomalies in ppb as a function of month and altitude over a mean seasonal cycle, plotted from the surface to 8 km (~330 hPa) in the NH for GEOSCCM (top row) and the NOAA empirical background (bottom row). From left to right: 10° latitude bins centered at 70°, 60°, 50° and 40°N. Monthly anomalies are computed by subtracting the annual mean value at each pressure level.

Figure 4 provides a further perspective on the signal of N_2O-poor stratospheric air in the NOAA empirical background. When viewed as a 12-month sequence of altitude-latitude contours, the signal originates at northern polar latitudes in the upper troposphere in late winter and early spring, descends and mixes equatorward, with a peak influence around August-September at middle to high latitudes in the NH. By late fall and winter, the signal has dissipated at the surface but is forming again in the upper troposphere.

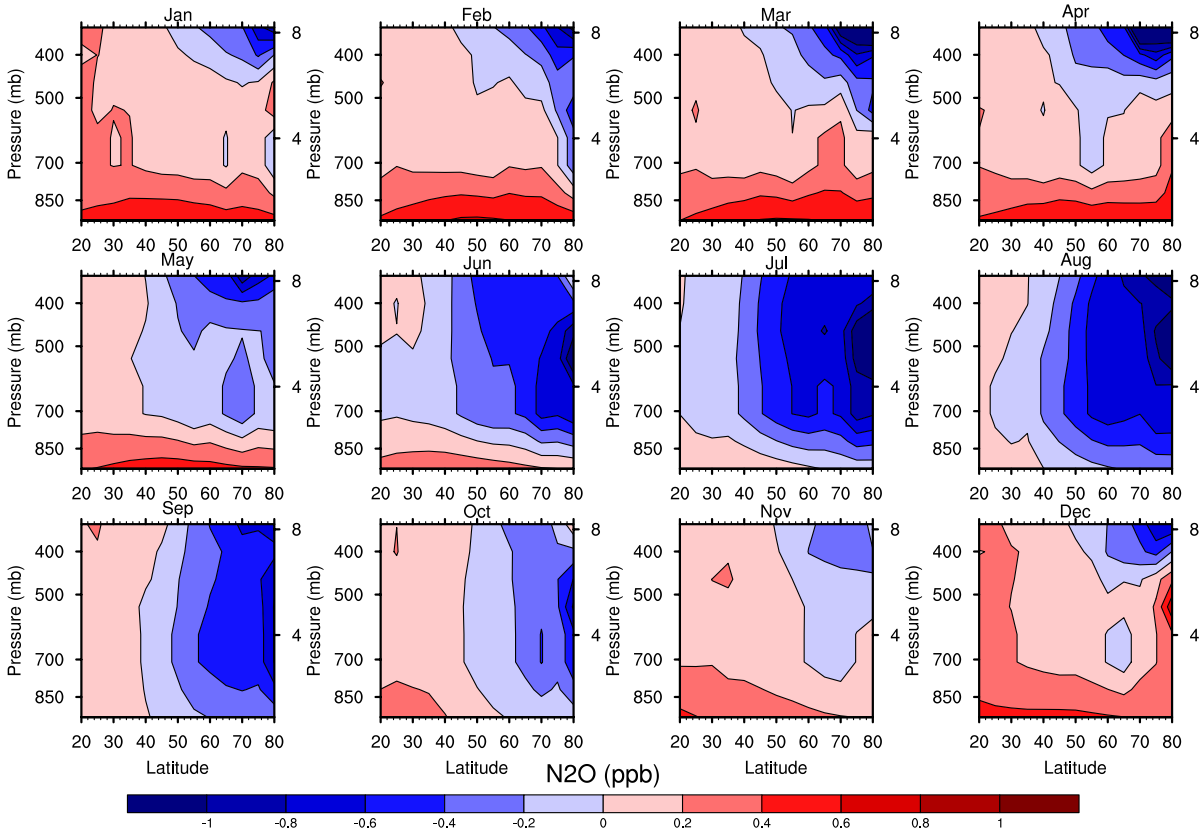

Figure 4: N_2O anomalies in the Northern Hemisphere from the NOAA empirical background, plotted in a monthly sequence of altitude vs. latitude plots extending from the surface up to 8 km (~330 hPa) and from 20°N-80°N.

QCLS N_2O data from airborne surveys extend up to 14 km and thus provide a broader perspective with respect to altitude of the stratospheric influence on tropospheric N_2O. Of the 3 airborne surveys available for our analysis (HIPPO, ORCAS and ATom), HIPPO provides the most complete N_2O time series across all seasons. In Figure 5, the southbound transects from the five HIPPO deployments are detrended and arranged chronologically as altitude-latitude contour plots over an annual mean cycle. These plots form a sequence with a similar movement of N_2O-poor stratospheric air from upper levels down to the surface as seen in GEOSCCM and the NOAA empirical boundary data. This progression is most readily seen in the NH in Figure 5, in which N_2O-poor air in the polar lower stratosphere has crossed the tropopause by March. By June it has descended into the middle troposphere and started moving equatorward, reaching its maximum influence at the surface in August. By October/November, the stratospheric signal is no longer visible at the surface following tropospheric mixing and dilution.

This seasonal progression is also evident in a fuller dataset that also includes the ATom and northbound HIPPO transects collapsed into a climatological cycle (Supplementary Figure S2)

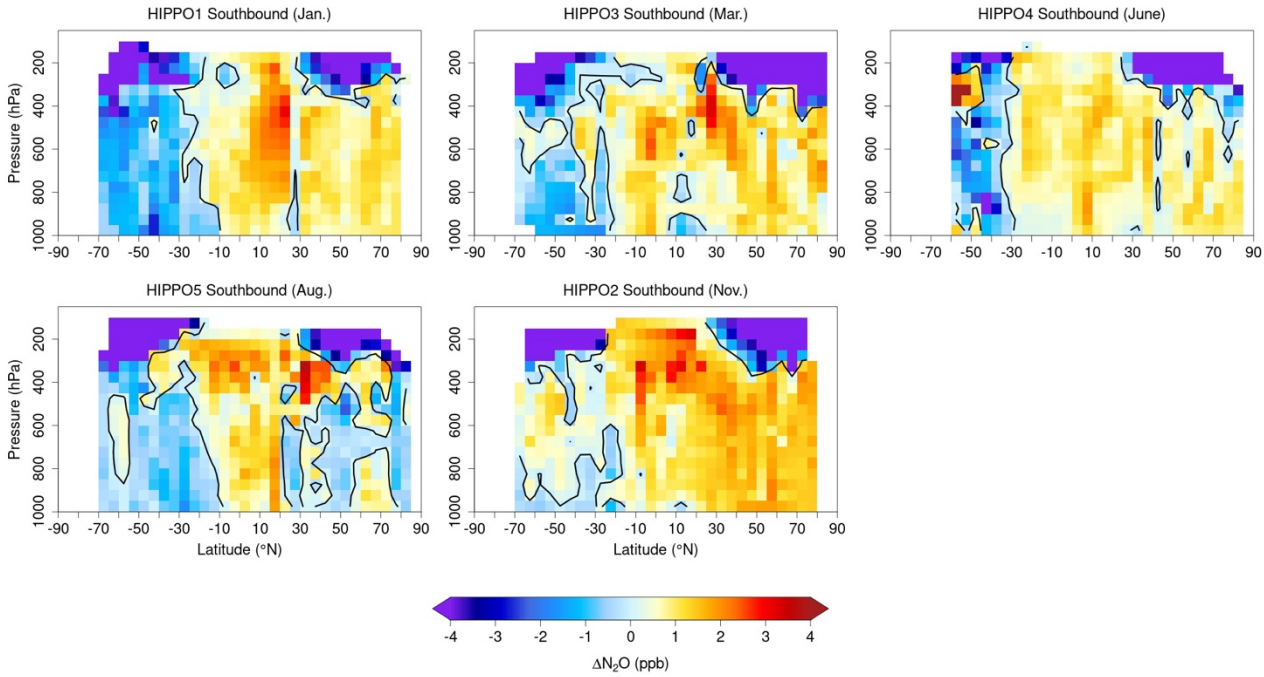

Figure 5: Sequence of five HIPPO pressure-latitude contour plots arranged to form an annual sequence an annual sequence; from left to right: January, March, June (top row) and August, November (bottom row). Each panel represents a north-to-south transect across latitude with vertical profiling from the surface to 14 km.

3.2 Correlation analysis of the Surface N_2O Atmospheric Growth Rate (AGR)

In this section NOAA surface N_2O AGR anomalies from 1998-2020 are plotted against polar lower stratospheric temperature (PLST) and QBO and ENSO indices, with varying lag times as described in the Methods. The analysis focuses on the NOAA global, NH, and SH mean products, with the premise that a significant correlation between the interannual variability in the N_2O AGR and one or more of the indices can be interpreted to support a causal influence of the latter on the N_2O AGR. A similar correlation analysis is performed for the GEOSCCM N_2O AGR and the model's internally-generated QBO and PLST fields, with the assumption that similarities between modeled and observed correlations may also support a causal influence.

Figure 6a shows that in the SH the QBO index is positively correlated to the NOAA observed surface N_2O AGR, with an optimal correlation (R = 0.42) for QBO in the upper stratosphere at 20 hPa with a time shift of about 19 (17-21) months relative to the N_2O time series. The correlation between GEOSCCM QBO and the SH N_2O AGR is weaker (R = 0.24) but also positive in sign in the upper stratosphere with a similar optimal shift in the GEOSCCM QBO of about 19 months (Figure 6c).

Spring PLST is not significantly correlated to the NOAA surface N_2O AGR in the SH (Figure 6b), but within GEOSCCM the two are negatively correlated (Figure 6d). The correlation with PLST in GEOSCCM occurs for the N_2O AGR averaged over a range of different 12-month intervals, with the strongest correlation (R = -0.61) over the 12-month interval from May-April (Figure 6d).

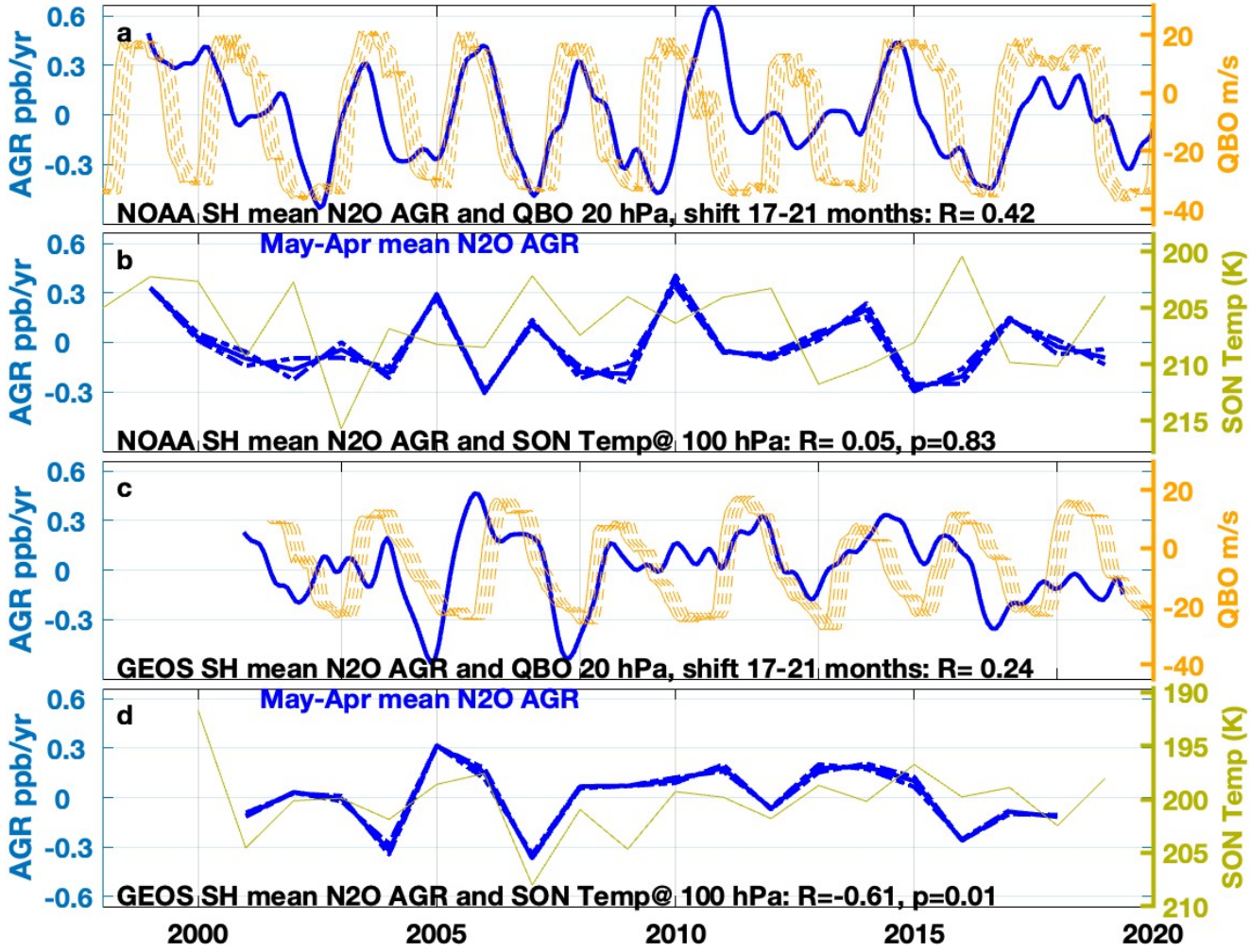

Figure 6: SH N_2O atmospheric growth rate (AGR) for (a) NOAA and (c) GEOSCCM plotted with the QBO index at 20 hPa with a 17-21 month forward shift in the index. (b,d) SH N_2O AGR plotted with mean lower stratospheric temperature averaged over 60-90°S for September-November in the year prior to the annual label on the X axis. The AGR is averaged from monthly N_2O data over the ensuing 12 month period May-April (solid blue line), shifted plus or minus 1 month (dotted blue lines), for (b) NOAA and (d) GEOSCCM. Note: to convert to %/yr (AGR units often used in the literature) ppb/yr can be multiplied by 100/323 (~1/3), where 323 is the mean tropospheric mixing ratio of N_2O over 1998-2020.

In contrast to the SH, the NOAA surface N_2O AGR in the NH is signficantly correlated to winter PLST (R = -0.61), with an optimal correlation for the 12-month period from July-June encompassing the January-March PLST average (Figure 7b). A similar correlation is found between the GEOSCCM PLST and NH N_2O AGR (Figure 7d). Also in contrast to the SH, the NOAA NH N_2O AGR is correlated only weakly to the QBO index at all altitudes, with a negative sign. The strongest correlation in the NH occurs for 50 hPa QBO (R= -0.23) with a 10-14 months lag (Figure 7a). GEOSCCM predicts

a stronger negative correlation (R = -0.47) between the GEOSCCM QBO and the NH N_2O AGR, which also is optimal around 50 hPa with 10-14 month QBO lag (Figure 7c).

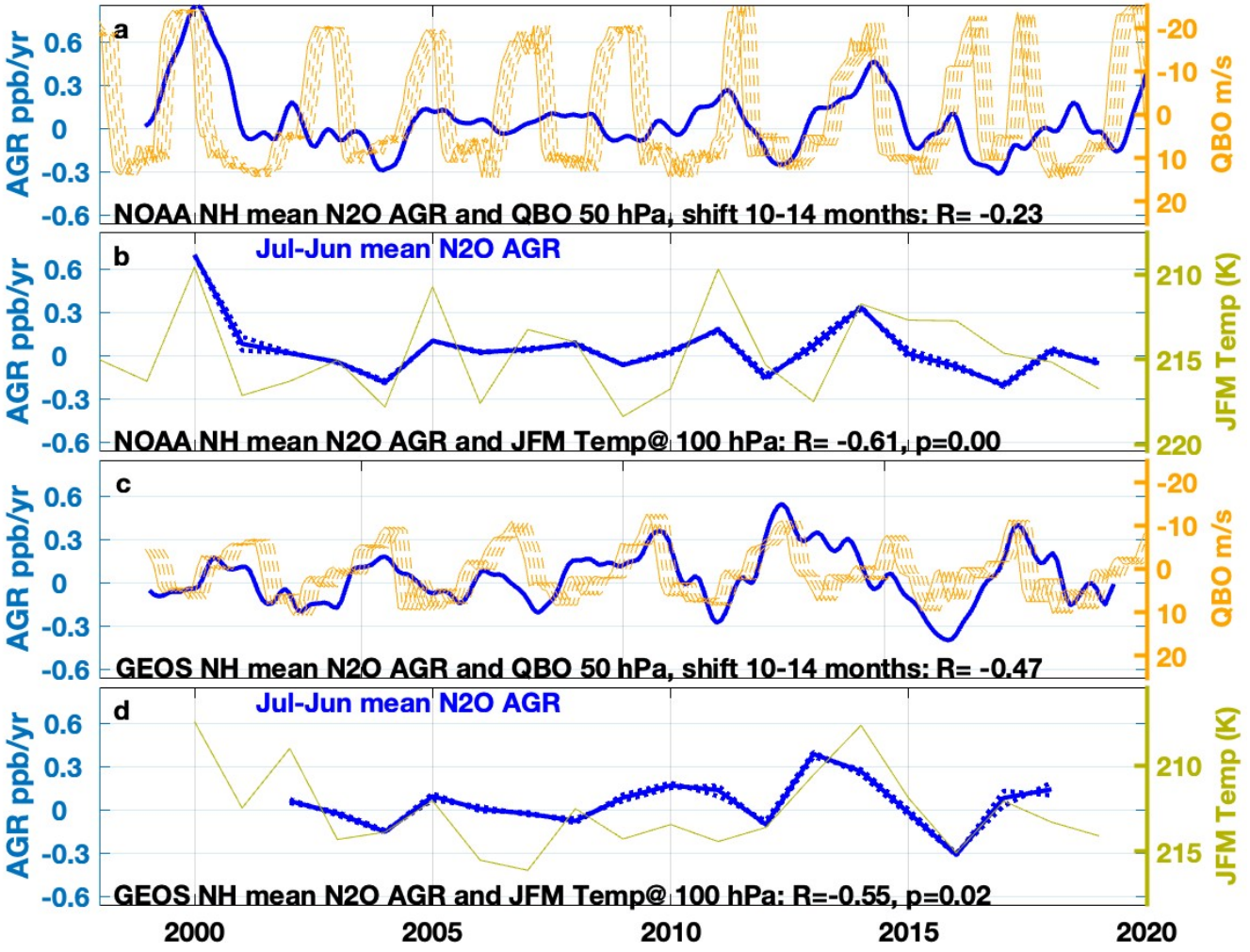

Figure 7: NH N_2O atmospheric growth rate (AGR) for (a) NOAA and (c) GEOSCCM plotted with the QBO index at 50 hPa with a 10-14 month forward shift in the index. (b,d) NH N_2O AGR plotted with mean lower stratospheric temperature averaged over 60-90°N for January-March of the year labeled on the X axis. The AGR is averaged from monthly N_2O data over the encompassing 12 month period July-June (solid blue line), shifted plus or minus 1 month (dotted blue lines), for (b) NOAA and (d) GEOSCCM.

The Niño 3.4 index is negatively correlated (R = -0.5) to the NOAA surface N_2O AGR both globally and in the SH, with little to no monthly lag in the index. In the NH, the correlation is weaker (R= -0.35)

with an optimal lag of 7 months in the Niño 3.4 index relative to the NOAA N_2O AGR (Figure 8).

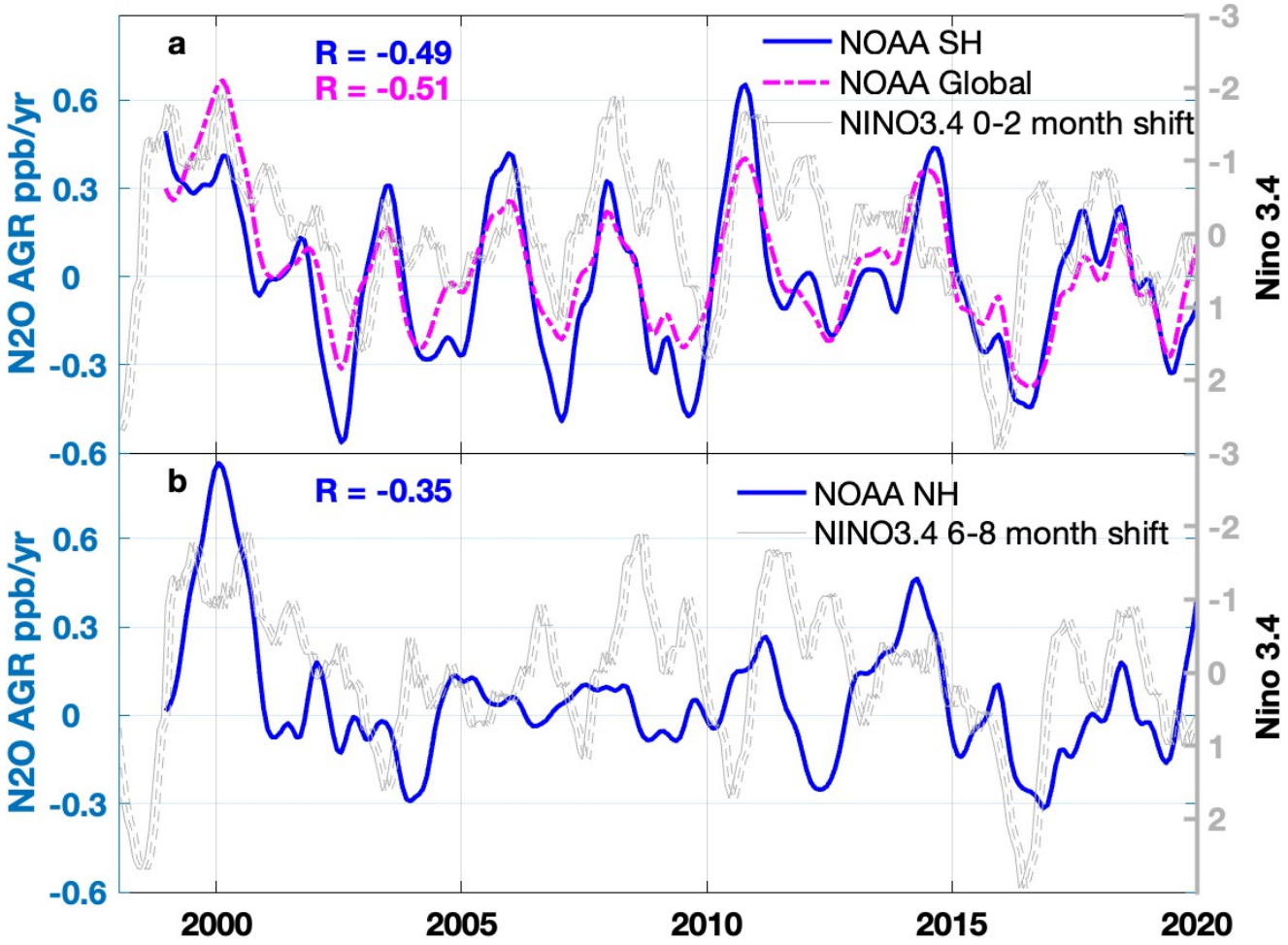

Figure 8: NOAA N_2O AGR plotted with the Nino3.4 index for a) SH and global mean AGR with a 0-2 month shift in the index and b) NH AGR with a 6-8 month shift in the index.

3.3 Correlation analysis of N_2O monthly anomalies

The N_2O monthly anomaly correlation analysis is focused solely on PLST, which has one unique value each year that can be plotted against the corresponding N_2O anomaly for any given month. The months selected for this correlation analysis were those surrounding the seasonal N_2O minimum, which is the most distinct feature of the seasonal cycle at remote mid and high latitude NOAA sites. These months were hypothesized, based on previous work, as most likely to be influenced by the descent of N_2O-poor

air from the stratosphere (*Nevison et al.*, 2011). In contrast, QBO and ENSO are monthly indices for which it is not straightforward to choose a representative month to correlate to the N_2O monthly anomaly, given that the anomaly might result from the cumulative effect over multiple months.

Figure 9 shows that in the SH, PLST from the previous spring is significantly negatively correlated to NOAA surface station N_2O monthly anomalies in austral summertime, when N_2O is descending into its autumn seasonal minimum (Figure 9a). This correlation is observed in January and February at several extratropical southern NOAA sites including Cape Grim, Tasmania, Palmer Station, Antarctica, and South Pole and is shown for February at South Pole in Figure 9b. The sign of the correlation is such that more negative surface N_2O anomalies occur during warm years, in which stronger than average descent of N_2O-poor air occurs into the polar lower stratosphere over the austral winter and spring. GEOSCCM simulates similar correlations between PLST and austral summer N_2O anomalies, both for N_2O_{ST} and total N_2O (Figure 9c,d) at these sites, although the correlations are strongest in February and March, i.e., delayed by about 1 month relative to NOAA surface observations.

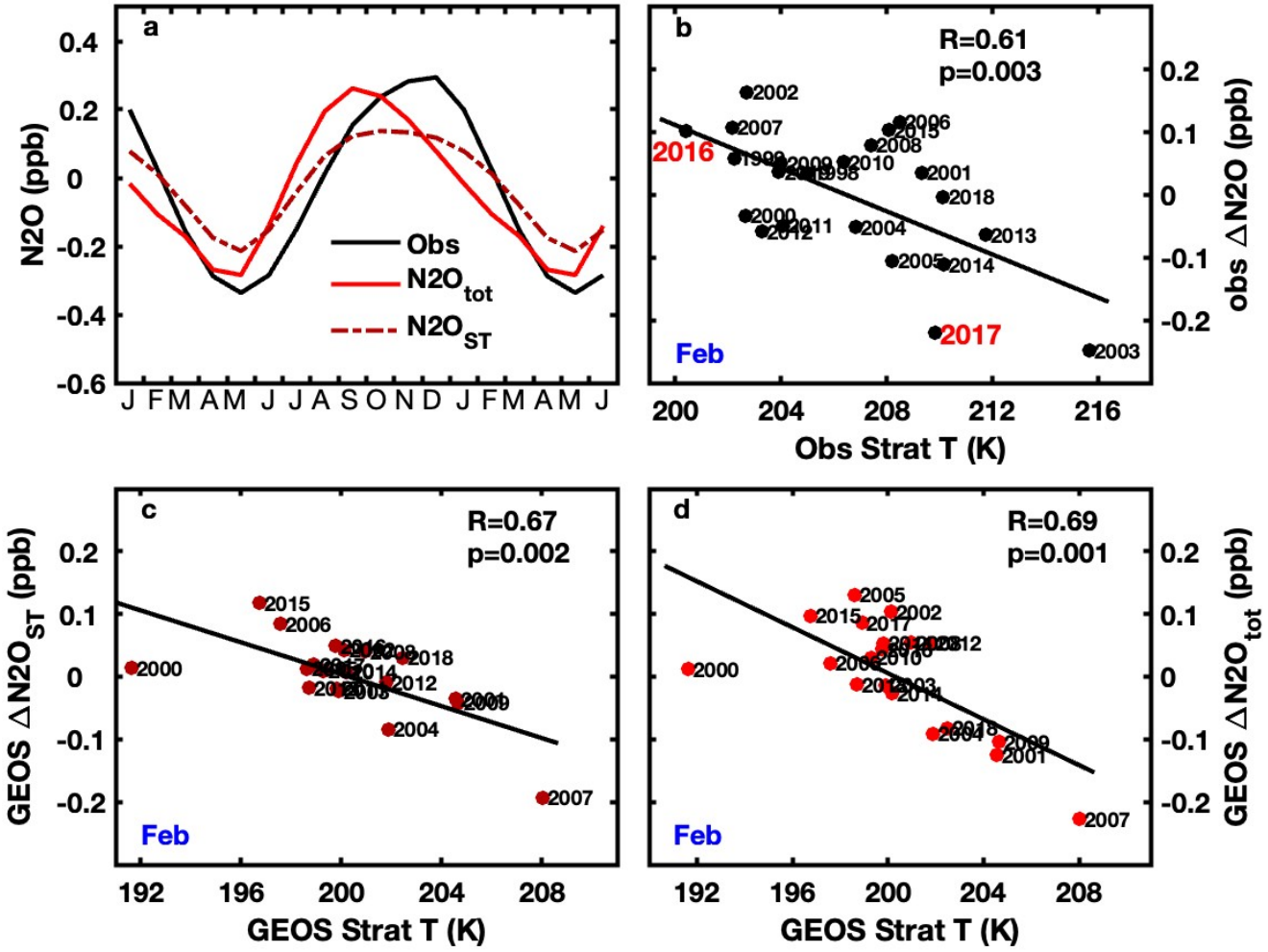

Figure 9: Top row shows a) South Pole mean seasonal cycle in N_2O for observed N_2O and GEOSCCM total N_2O and N_2O_{ST} and b) NOAA surface N_2O seasonal anomalies in February at South Pole spanning 1998-2020, plotted vs. mean lower stratospheric MERRA-2 temperature at 100 hPa averaged over 60-90°S over the previous spring (September-November). The labeled anomalies in 2016 and 2017 correspond to the year of the ORCAS and ATom-2 aircraft surveys, respectively. Bottom row shows GEOSCCM seasonal anomalies for c) N_2O_{ST} and d) total N_2O in February at South Pole spanning 2000-2019, plotted vs. mean GEOSCCM lower stratospheric temperature, which is sampled the same way as the MERRA-2 temperature.

Figure 10, which compares February altitude-latitude N_2O contour plots from the ORCAS and ATom airborne surveys, offers support for the observed surface correlations in Figure 9. The contour plots show more depleted N_2O values in the extratropical SH during ATom-2, which took place in February 2017 after a relatively warm spring in the Antarctic lower stratosphere (strong BDC), compared to ORCAS, which took place in January-February 2016 after a particularly cold spring (weak BDC). The right panel shows ATom-2 data over the full 65˚S to 75˚N latitude span, putting the stratospheric

influence coming from the southern polar stratosphere into broader perspective. The left panel extends only from 70˚S to 20˚S because ORCAS was confined to that region.

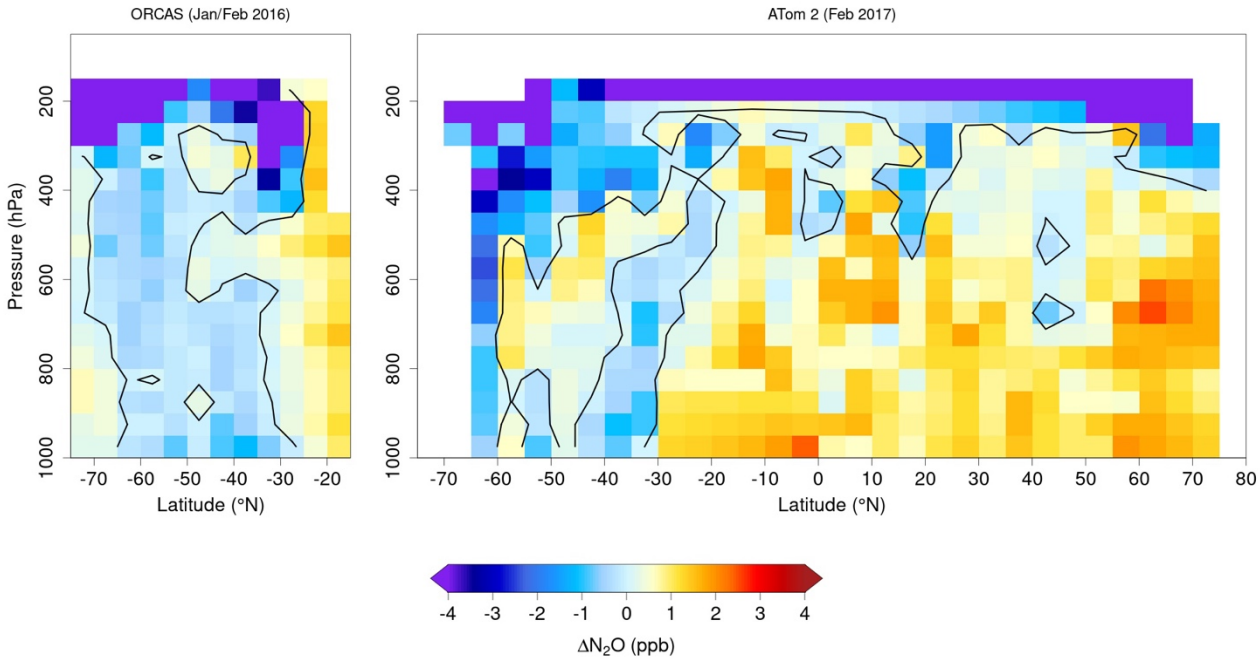

Figure 10. N_2O anomlies in ppb as a function of altitude and latitude from (left panel) ORCAS (Jan.-Feb. 2016) and (right panel) ATom-2 (Jan.-Feb. 2017).

In contrast to the SH, PLST in the NH from the previous winter is not correlated significantly to N_2O monthly anomalies at extratropical NOAA surface sites in any of the months surrounding the NH N_2O seasonal minimum. GEOSCCM also does not predict significant correlations between PLST and summer N_2O anomalies at most northern NOAA sites, with the exception of Mace Head, Ireland (MHD), where a negative correlation is found in July (Supplementary Figure S3).

4. Discussion

The atmospheric N_2O observations and model results assembled here present several new lines of evidence that the stratosphere helps drive the seasonal minimum in tropospheric N_2O and also influences its atmospheric growth rate. First, the vertical cross sections of atmospheric N_2O from

aircraft provide a broad-scale perspective, in which N_2O-poor air shows up in the winter polar lower stratosphere, crosses the tropopause around the time of polar vortex breakup, and descends downward and equatorward, reaching Earth's surface by summer or early fall. These patterns are seen in both the NOAA empirical background and in global airborne survey data (Figures 3, 4, 5). Second, GEOSCCM simulations show similar 3-dimensional patterns to those in the NOAA empirical background (Figure 4) as well as correlations between the surface N_2O AGR with internally modeled QBO and PLST indices that are similar to those found in observations (Figures 6, 7). In addition, GEOSCCM predicts correlations between February N_2O anomalies and PLST in the SH, both for total N_2O, similar to those observed, and for the explicitly resolved stratospheric N_2O tracer N_2O_{ST} (Figure 9).

The comparison of GEOSCCM output to NOAA observations, while supporting a stratospheric influence on the troposphere, also raises questions. The phasing of the GEOSCCM N_2O seasonal cycle is delayed relative to observations, especially in the NH, and the model simulates too long a delay in propagating stratospheric signals down to the surface (Figure 1,3). The rate of descent in the stratosphere has been shown to be underestimated in atmospheric models (e.g. *Brühl et al.*, 2007; *Khosrawi et al.*, 2009; 2018) and this may also be the case in the troposphere. Another issue is that the seasonality of surface N_2O emissions may not be well represented in the GEOSCCM simulation, e.g., summer soil emissions may be overestimated, leading to unrealistic surface maxima in July (*Liang et al.*, 2022).

With respect to the aircraft data, the NOAA empirical background and QLCS vertical cross sections, while showing similar features, are not matched exactly for comparison. QCLS data are measured across a narrow longitude band of the flight track for any given latitude on a limited number of days, while the NOAA empirical background is shown as a monthly mean, zonally averaged across most of the western hemisphere (170°-50°W). Consequently, QCLS data are more likely to display synoptic-scale variability, such as the apparent surface source plumes over the Southern Ocean seen in Figure 10.

4.1 Correlation to stratospheric indices: signs and magnitudes

The results of the correlation analysis based on NOAA surface N_2O data are similar to those found in previous studies based on Advanced Global Atmospheric Gases Experiment (AGAGE) surface N_2O data (*Prinn et al*., 2000; *Nevison et al*., 2007; 2011). In general, these correlations are weak, in part because the variability in surface N_2O is very small compared to its mean tropospheric mixing ratio. Nevertheless, PLST in the NH correlates significantly to NOAA surface N_2O AGR anomalies (Figure 7b) and PLST in the SH correlates significantly to monthly N_2O anomalies in February near the time of the seasonal N_2O minimum (Figure 9b). The negative sign of these correlations is easily understood and consistent with more transport of warm, N_2O-poor air into the polar lower stratosphere in years with stronger BDC, with subsequent cross-tropopause transport that deepens the descent of N_2O into its seasonal minimum and slows the observed AGR of N_2O at the surface.

The reason for the positive correlation of the QBO index with the SH surface N_2O AGR (Figure 6a,c) is less obvious. A similar correlation in the SH, but not the NH, has been observed in other studies *Ray et al.* (2020) but not fully explained. In our analysis, the positive correlation between the QBO and the SH N_2O AGR is strongest for the QBO at 20 hPa with 17-19 months lag and then weakens with decreasing QBO altitude down to 100 hPa, with a concurrent decrease in the optimal lag, likely due to the time needed for downward propagation of QBO winds (Supplementary Figure S4). At 50 hPa, we find an optimal lag time of 10-12 months (R = +0.33), consistent with *Ray et al.* (2020).

Photochemical destruction of N_2O is highest when QBO winds above 30 hPa are in the westerly (positive) phase and lower altitude QBO winds are in the easterly (negative) phase. This configuration is associated with increased vertical upwelling in the tropical lower stratosphere, which transports more N_2O to its peak loss region around 32 km (*Strahan et al.*, 2021; *Ruiz et al.*, 2021). Thus the magnitude of QBO-associated photochemical destruction per se cannot be the main driver of the stratospheric influence on surface N_2O, since one would logically expect a negative correlation (i.e., slower growth in the troposphere due to more stratospheric N_2O loss during positive QBO). *Ruiz et al.* (2021) similarly concluded that surface variability in N_2O is not correlated directly to the QBO-driven variability in

stratospheric loss, but rather by dynamical variations in cross tropopause fluxes of air, which are governed at least in part by the BDC.

The dynamics of the QBO, its interaction with the BDC and ultimate influence on surface N_2O are complex. However, the positive correlation of QBO, peaking at 20 hPa, with the SH N_2O AGR, could be explained in the context of *Strahan et al.* (2015), as described in detail in the Supplementary Materials, Section S1. Briefly, the QBO has an associated meridional circulation, which transports N_2O-poor air poleward from the region of peak photochemical destruction in the tropics between about 30 hPa to 10 hPa in altitude. Paradoxically, this meridional circulation transports less N_2O-poor air toward the poles during the phase when the QBO is positive above 30 hPa. The N_2O-poor air subsequently is trapped in the Antarctic polar vortex and undergoes BDC-driven diabatic descent, in isolation from mixing with lower latitudes, arriving largely intact in the lower stratosphere and eventually at earth's surface, with a long lag time consistent with the 17-19 month lag found in Figure 9a.

4.2 Northern vs. southern hemisphere differences

In the NH, the planetary wave activity that drives the BDC is stronger due to the more variable topography and stronger land-sea contrasts. Consequently, the BDC-driven descent into the winter pole is more strongly seasonal and the NH polar vortex is less isolated (*Scaife and James*, 2000, *Kidston et al.*, 2015), such that any signal associated with the QBO meridional circulation does not transport intact to lower altitudes (*Strahan et al.*, 2015). This may explain why, for both NOAA surface stations and GEOSCCM, the NH N_2O AGR is more strongly correlated to PLST (a proxy for the BDC) than it is to the QBO, consistent with *Ruiz et al.* (2021).

In contrast to the NH, the NOAA SH surface N_2O AGR does not correlate to PLST. This result is somewhat puzzling given the significant correlation between PLST and NOAA N_2O February anomalies at SH high latitude surface sites (Figure 9), which are supported by the ATom-2 and ORCAS data (Figure 10). It appears that the impact of the stratosphere in austral summer as tropospheric N_2O

descends into its seasonal minimum is not sufficient to influence the N_2O AGR across the whole SH over the entire year. The SH N_2O AGR results may reflect the strong preservation of the QBO signal that is ultimately transported into the troposphere, as discussed above, combined with the relatively weaker BDC in the SH and/or the interference of ENSO-driven signals discussed below.

4.3 Correlations with ENSO

The NOAA surface station N_2O AGR correlation with ENSO indices is similar in magnitude to the correlations with stratospheric indices in the SH (R = -0.49, 0-2 month phase shift) and relatively weaker in the NH (R=-0.35, 7 month optimal phase shift) (Figure 10). The correlation in the SH could in part reflect meteorological shifts in the tropical low level convergence pattern during positive ENSO (El Niño) conditions. For atmospheric gases with a positive north-south latitudinal gradient, these shifts result in a lessened influence of winds from the NH on the tropical SH and an increased influence of southeasterly winds. The NOAA Samoa site at 14°S, which strongly influences the cosine-latitude-weighted SH average, is known to be affected by these kinds of wind shifts (*Prinn et al.*, 1992; *Nevison et al.*, 2007). The fact that the N_2O AGR correlation with ENSO is considerably weaker in the NH than in the SH suggests a limited impact of ENSO on NH N_2O and supports the hypothesis that reduced north-to-south transport during positive ENSO contributes to the correlation observed in the SH.

The negative correlation between N_2O AGR and ENSO also may reflect a true reduction in the biogeochemical N_2O source during the positive ENSO phase, for example, due to drought over tropical land or due to reduced upwelling in the tropical ocean (*Ishijima et al.*, 2009; *Thompson et al.*, 2013). The most well documented biogeochemical response of N_2O to ENSO events occurs in the Eastern Tropical South Pacific (ETSP), a well known oxygen minimum zone (OMZ) and hot spot of oceanic N_2O emissions (*Arévalo-Martínez*, 2015; *Ji et al*., 2019). El Niño conditions decrease upwelling in the ETSP, thereby reducing the surface productivity, deepening the oxycline, contracting the OMZ and decreasing the N_2O sea-to-air flux (*Ji et al.*, 2019; *Babbin et al.*, 2015).

However, less than one quarter of the total N_2O budget likely comes from oceanic emissions, of which the ETSP is only one component (*Yang et al.*, 2020; *Canadell et al.*, 2021). This raises questions about whether a reduced ETSP source (or a strengthened source during La Niña periods) has enough leverage to control the overall N_2O AGR. *Ruiz et al.* (2021) removed the stratospheric influence from surface N_2O data to tease out a source of ~ 1 Tg N (about 5% of the total annual N_2O source) associated with the 2010 La Niña event, which could have come from tropical land or ocean, or some combination of both. Similarly, *Kort et al.* (2011) found evidence of strong episodic pulses of ~ 1 Tg N from tropical regions, based on maxima in QCLS N_2O data measured in the middle and upper troposphere during aircraft campaigns in 2009. These pulses were not tied specifically to an ENSO event but rather more generally demonstrated the strength of the tropical N_2O source.

5 Summary and **Conclusions**

N_2O observations from aircraft provide direct evidence for a stratospheric influence on tropospheric N_2O that previously was inferred based on correlations of surface N_2O data to stratospheric indices. GEOSCCM simulations corroborate the view that N_2O-poor air descends throughout the winter into the polar lower stratosphere, crosses the tropopause in spring or early summer, and descends downward and equatorward, transmitting a diluted but still coherent signal to Earth's surface in late summer to early autumn (August-September in the NH, April-May in the SH). In support of this view and consistent with previous studies, significant correlations are found between the N_2O AGR observed at long-term NOAA surface monitoring sites and either the QBO index in the SH or PLST in the NH, where PLST is a proxy for the strength of the BDC. Correlations between the N_2O AGR and ENSO indices are also significant in the SH, suggesting a joint influence of ENSO and the stratosphere on the AGR in that hemisphere. The QBO influences the rate at which N_2O is transported to and destroyed in the tropical middle to upper stratosphere, but complex atmospheric dynamics buffer how variations in the stratospheric N_2O loss rate are transmitted across the tropopause to modulate the surface N_2O AGR. Cross-tropopause transport in polar regions is linked closely to the BDC and appears to be a more direct influence than the QBO on the N_2O AGR in the NH. In contrast, in the SH, the combination of a better-preserved QBO signal and weaker BDC may lead to a direct (albeit with a ~1.5 year lag) correlation

between the QBO and the SH N_2O surface AGR, consistent with current knowledge of stratospheric dynamics. To further refine our understanding of variability in tropospheric N_2O, long-term monitoring at surface and aircraft-based sites is essential and would be complemented by more global airborne surveys extending into the lower stratosphere. The latter provide new insights into stratospheric influences on tropospheric N_2O and advance our ability to interpret and quantify surface N_2O sources.

Code Availability

Codes are available from the corresponding author upon request.

Data Availability

NOAA N_2O data can be obtained by contacting xin.lan@noaa.gov or through the NOAA Global Monitoring Laboratory at https://gml.noaa.gov/aftp/data/trace_gases/n2o/flask/. QCLS N_2O data are openly available and archived in the Oak Ridge National Laboratory Distributed Active Archive Center (ORNL DAAC) https://doi.org/10.3334/ORNLDAAC/1925 (ATom), and at the National Center for Atmospheric Research (NCAR) https://doi.org/10.5065/D6SB445X (ORCAS) and https://doi.org/10.3334/CDIAC/HIPPO_010 (HIPPO).

Author contributions

CDN designed and carried out the analysis and prepared the main manuscript and most of the figures. QL implemented separate stratospheric and tropospheric N_2O tracers in GEOSCCM and provided model output. PN computed QBO indices and MERRA stratospheric temperatures and provided guidance on stratospheric dynamics. BBS, RC, YG and EK provided QCLS N_2O data and BBS created contour plots of the QCLS data. XL and GD provided N_2O surface data. All authors reviewed and approved the manuscript.

Competing Interests

The authors declare they have no conflicts of interest.

Acknowledgments

CDN and QL acknowledge support from the NASA MAPS program (award 16-MAP16-0049). The authors are grateful to Arlyn Andrews, Colm Sweeney, Bradley Hall, Ed Dlugokencky, Steve Wofsy, Bruce Daube, and many others who have made this study possible, through collection and analysis of surface station and NOAA aircraft flasks, in situ NOAA station measurements, and QCLS aircraft campaign observations. The HIPPO and ORCAS observations, and the contributions of BBS were supported by the National Center for Atmospheric Research, which is a major facility sponsored by the National Science Foundation under Cooperative Agreement No. 1852977.

References

Akima, H.: A Method of Bivariate Interpolation and Smooth Surface Fitting for Irregularly Distributed Data Points, ACM Transactions on Mathematical Software, Vol. 4, No. 2, June 1978, pp. 148-159. Copyright 1978, Association for Computing Machinery, Inc, 1978

Arévalo-Martínez, D. L., Kock, A., Löscher, C. R., Schmitz, R. A. & Bange, H. W.: Massive nitrous oxide emissions from the tropical South Pacific Ocean. Nat. Geosci., 8, 530, 2015.

Babbin, A.R., Bianchi, D., Jayakumar, A, and Ward, B. B.: Rapid nitrous oxide cycling in the suboxic ocean, Science, 348, doi:10.1126/science.aaa8380, 2015.

Baldwin, M.P., Gray, L.J., Dunkerton, T.J., Hamilton, K., Haynes, P.H., Randel, W.J., Holton, J.R., Alexander, M.J., Hirota, I., Horinouchi, T., Jones, D.B.A., Kinnersley, J.S., Marquardt, C., Sato, K., Takahashi, M., The quasi-biennial oscillation, Reviews of Geophysics, 39(2), 179-229, 2001.

Bouwman, A.F. and Taylor, J.A.: Testing high-resolution nitrous oxide emission estimates against observations using an atmospheric transport model, Global Biogeochem. Cy., 10, 307-318, 1996.

Bouwman, A.F., van der Hoek, K.W., and Olivier, J.G.J.: Uncertainties in the global source distribution of nitrous oxide, J. Geophys. Res., 100, 2785-2800, 1995.

Brühl, C., Steil, B., Stiller, G., Funke, B., and Jöckel, P.: Nitrogen compounds and ozone in the stratosphere: comparison of MIPAS satellite data with the chemistry climate model ECHAM5/MESSy1, Atmos. Chem. Phys., 7, 5585–5598, https://doi.org/10.5194/acp-7-5585-2007, 2007.

Butchart, N.: Reviews of Geophysics The Brewer-Dobson circulation, Rev. Geophys, 52, 157–184. https://doi.org/10.1002/2013RG000448, 2014.

Canadell, J. G., P. M. S. Monteiro, M. H. Costa, L. Cotrim da Cunha, P. M. Cox, A. V. Eliseev, S. Henson, M. Ishii, S. Jaccard, C. Koven, A. Lohila, P. K. Patra, S. Piao, J. Rogelj, S. Syampungani, S. Zaehle, K. Zickfeld, 2021, Global Carbon and other Biogeochemical Cycles and Feedbacks. In: Climate Change 2021: The Physical Science Basis. Contribution of Working Group I to the Sixth Assessment Report of the Intergovernmental Panel on Climate Change (Masson-Delmotte, V., P. Zhai, A. Pirani, S. L. Connors, C. Péan, S. Berger, N. Caud, Y. Chen, L. Goldfarb, M. I. Gomis, M. Huang, K. Leitzell, E. Lonnoy, J.B.R. Matthews, T. K. Maycock, T. Waterfield, O. Yelekçi, R. Yu and B. Zhou (eds.)). Cambridge University Press. In Press.

Earth Systems Research Laboratory, Multivariate ENSO Index (MEI). NOAA (2017).

Elkins, J.W, and Dutton, G.S.: Nitrous oxide and sulfur hexafluoride (in 'State of the Climate in 2008'), Bull. Amer. Meteor. Soc, 90, S38-S39, 2009.

Forster, P., Ramaswamy, V., Artaxo, P., Berntsen, T., Betts, R., Fahey, D.W., Haywood, J., Lean, J., Lowe, D.C., Myhre, G., Nganga, J., Prinn, R., Raga, G., Schulz, M. and Van Dorland, R.: Changes in Atmospheric Constituents and in Radiative Forcing. In: Climate Change 2007: The Physical Science Basis. Contribution of Working Group I to the Fourth Assessment Report of the Intergovernmental Panel on Climate Change. Cambridge University Press Cambridge, United Kingdom and New York, NY, USA, 2007.

Gonzalez, Y., Commane, R., Manninen, E., Daube, B.C., Schiferl, L., McManus, J.B., McKain, K, Hintsa, E.J., Elkins, J.W., Montzka, S.A., Impact of stratospheric air and surface emissions on

tropospheric nitrous oxide during ATom, Atmospheric Chemistry and Physics Discussions, https://doi.org/10.5194/acp-2021-167, 2021.
Gurney, K. R., Law, R.M., Denning, A.S., Rayner, P.J., Pak, B.C., Baker, D.F., Bousquet, P., Bruhwiler, L., Chen, Y.-H., Ciais, P., Fung, I.Y., Heimann, M., John, J., Maki, T., Maksyutov, S., Peylin, P., Prather, M., Taguchi, S.: Transcom 3 inversion intercomparison: Model mean results for the estimation of seasonal carbon sources and sinks, Global Biogeochem. Cycles, 18, GB1010, doi:10.1029/2003GB002111, 2004.
Hall, B. D., Dutton, G.S., and Elkins, J. W.: The NOAA nitrous oxide standard scale for atmospheric observations, J. Geophys. Res., 112, D09305, doi:10.1029/2006JD007954, 2007.
Hall, B. D., Dutton, G. S., Mondeel, D. J., Nance, J. D., Rigby, M., Butler, J. H., Moore, F. L., Hurst, D. F. and Elkins, J. W.: Improving measurements of SF_6 for the study of atmospheric transport and emissions, Atmos. Meas. Tech., 4, 2441-2451, doi: 10.5194/amt-4-2441-2011, 2011.
Hammerling, D. M., Michalak, A. M., Kawa, S. R.: Mapping of CO_2 at High Spatiotemporal Resolution using Satellite Observations: Global Distributions from OCO-2, Journal of Geophysical Research, 117, D06306, doi:10.1029/2011JD017015, 2012.
Hirsch, A.I., Michalak, A.M., Bruhwiler, L.M., Peters, W., Dlugokencky, E.J. and Tans, P.P.: Inverse modeling estimates of the global nitrous oxide surface flux from 1998-2001, Global Biogeochem. Cy., 20, GB1008, doi:10.1029/2004GB002443, 2006.
Holton, J.R., Haynes, P.H., McIntyre, M.E., Douglass, A.R., Rood, R.B. and Pfister, L.: Stratosphere-troposphere exchange, Rev. Geophys., 33(4), 403-439, 1995.
Holton, J.: An Introduction to Dynamic Meteorology, no. v. 1 in An Introduction to Dynamic Meteorology, Elsevier Science, available at: https://books.google.be/books?id=fhW5oDv3EPsC (last access: 28 October 2020), 2004.
Huang, J., Golombek, A., Prinn, R., Weiss, R., Fraser, P., Simmonds, P., Dlugokencky, E.J., Hall, B., Elkins, J., Steele, P., Langenfelds, R., Krummel, P., Dutton, G., and Porter, L.: Estimation of regional emissions of nitrous oxide from 1997 to 2005 using multinetwork measurements, a chemical transport model, and an inverse method, J. Geophys. Res. 113, D17313, doi:10.1029/2007JD009381, 2008.
Ishijima, K., Patra, P.K., Takigawa, M., Machida, T., Matsueda, H., Sawa, Y., Steele, L.P., Krummel, P.B., Langenfelds, R.L., Aoki, S. and Nakazawa, T.: The stratospheric influence on the seasonal cycle of nitrous oxide in the troposphere as deduced from aircraft observations and model simulations, J. Geophys. Res., 115, D20308, doi:10.1029/2009JD013322, 2010.
Ji, Q., Babbin, A.R., Jayakumar, A., Oleynik, S. and Ward, BB.: 2015: Nitrous oxide production by nitrification and denitrification in the Eastern Tropical South Pacific oxygen minimum zone. Geophysical Research Letters, 42(24), 10,755–10,764, doi:10.1002/2015gl066853.
Ji, Q. et al.: Investigating the effect of El Niño on nitrous oxide distribution in the eastern tropical South Pacific. Biogeosciences, 16(9), 2079–2093, doi:10.5194/bg-16-2079-2019, 2019.
Jiang, X, Ku, W.L., Shia, R.-L., Li, Q., Elkins, J.W., Prinn, R.G., Yung, Y.L.: Seasonal cycle of N_2O: Analysis of data, Global Biogeochem. Cy., 21, GB1006, doi:10.1029/2006GB002691, 2007.
Jin, X. and Gruber, N.: Offsetting the radiative benefit of ocean iron fertilization by enhancing N_2O emissions, Geophys. Res. Lett. 30(24), 2249, 2003.
Jin, X., Najjar, R.G., Louanchi, F., and Doney, S.C.: A modeling study of the seasonal oxygen budget of the global ocean, J. Geophys. Res., 112, C05017, doi:10.1029/2006JC003731, 2007.

Kalnay, E., Kanamitsu, M., Kistler, R., Collins, W., Deaven, D., Gandin, L., Iredell, M., Saha, S., White, G., Woollen, J., Zhu, Y., Leetmaa, A., Reynolds, R., Chelliah, M., Ebisuzaki, W., Higgins, W., Janowiak, J., Mo, K.C., Ropelewski, C., Wang, J., Jenne, R., Joseph, D.: The NMC/NCAR 40-year reanalysis project, B. Am. Meteorol. Soc., 77, 437– 471, 1996.

Khosrawi, F., Kirner, O., Stiller, G., Höpfner, M., Santee, M. L., Kellmann, S., and Braesicke, P.: Comparison of ECHAM5/MESSy Atmospheric Chemistry (EMAC) simulations of the Arctic winter 2009/2010 and 2010/2011 with Envisat/MIPAS and Aura/MLS observations, Atmos. Chem. Phys., 18, 8873–8892, https://doi.org/10.5194/acp-18-8873-2018, 2018.

Khosrawi, F., Müller, R., Urban, J., Proffitt, M. H., Stiller, G., Kiefer, M., Lossow, S., Kinnison, D., Olschewski, F., Riese, M., and Murtagh, D.: Assessment of the interannual variability and influence of the QBO and upwelling on tracer–tracer distributions of N2O and O3 in the tropical lower stratosphere, Atmos. Chem. Phys., 13, 3619–3641, https://doi.org/10.5194/acp-13-3619-2013, 2013.

Khosrawi, F., Müller, R., Urban, J., Proffitt, M. H., Stiller, G., Kiefer, M., Lossow, S., Kinnison, D., Olschewski, F., Riese, M., and Murtagh, D.: Assessment of the interannual variability and influence of the QBO and upwelling on tracer–tracer distributions of N2O and O3 in the tropical lower stratosphere, Atmos. Chem. Phys., 13, 3619–3641, https://doi.org/10.5194/acp-13-3619-2013, 2013.

Kidston, J., Scaife, A., Hardiman, S. et al. Stratospheric influence on tropospheric jet streams, storm tracks and surface weather. Nature Geosci 8, 433–440 (2015). https://doi.org/10.1038/ngeo2424

Kort, E. A., Patra, P. K., Ishijima, K., Daube, B. C., Jiménez, R., Elkins, J.W., Hurst, D., Moore, F. L., Sweeney, C. and Wofsy, S. C.: Tropospheric distri- bution and variability of N2O: Evidence for strong tropical emissions, Geophys. Res. Lett., 38, L15806, doi:10.1029/2011GL047612, 2011.

Kroeze, C., Mosier, A. and Bouwman, L.: Closing the global N_2O budget: A retrospective analysis 1500-1994, Global Biogeochemical Cycles, 13, 1-8, 1999.

Lambert, A., Read, W. G., Livesey, N. J., Santee, M.L., Manney, G.L., Froidevaux, L., Wu, D.L., Schwartz, M.J., Pumphrey, H.C., Jimenez, C., Nedoluha, G.E., Cofield, R.E., Cuddy, D.T., Daffer, W.H., Drouin, B.J., Fuller, R.A., Jarnot, R.F., Knosp, B.W., Pickett, H.M., Perun, V.S., Snyder, W.V., Stek, P.C., Thurstans, R.P., Wagner, P.A., Waters, J.W., Jucks, K.W., Toon, G.C., Stachnik, R.A., Bernath, P.F., Boone, C.D., Walker, K.A., Urban, J., Murtagh, D., Elkins, J.W., Atlas, E.: Validation of the Aura Microwave LihPa Sounder middle atmosphere water vapor and nitrous oxide measurements, J. Geophys. Res., 112, D24S36, doi:10.1029/2007JD008724, 2007.

Lan, X., Dlugokencky, E.J., Mund, J.W., Crotwell, A.M., Crotwell, M.J., Moglia, E., Madronich, M., Neff, D. and Thoning, K.W.: Atmospheric Nitrous Oxide Dry Air Mole Fractions from the NOAA GML Carbon Cycle Cooperative Global Air Sampling Network, 1997-2021, Version: 2022-11-21, https://doi.org/10.15138/53g1-x417, 2022.

Lan, X., Tans, P., Thoning, K., & NOAA Global Monitoring Laboratory. (2023). NOAA Greenhouse Gas Marine Boundary Layer Reference - N2O. (Data set). NOAA GML. https://doi.org/10.15138/83W5-DK71.

Liang, Q., Stolarski, R.S., Douglass, A.R., Newman, P.A. and Nielsen, J.E.: Evaluation of emissions and transport of CFCs using surface observations and their seasonal cycles and the GEOS CCM

simulation with emissions-based forcing, J. Geophys. Res., 113, D14302, doi:10.1029/2007JD009617, 2008.
Liang, Q., Douglass, A.R., Duncan, B.N., Stolarski, R.S. and Witte, J.C.: The governing processes and timescales of stratosphere-to-troposphere transport and its contribution to ozone in the Arctic troposphere, Atmos. Chem. Phys., 9, 3011-3025, 2009.
Liang, Q., Nevison, C., Dlugokencky, E., Hall, B. D., & Dutton, G.: 3-D atmospheric modeling of the global budget of N_2O and its isotopologues for 1980–2019: The impact of anthropogenic emissions. Global Biogeochemical Cycles, 36, e2021GB007202. https://doi.org/10.1029/2021GB007202, 2022.
Lickley, M., Solomon, S., Kinnison, D., Krummel, P., Mühle, J., O'Doherty, S., et al.: Quantifying the imprints of stratospheric contributions to interhemispheric differences in tropospheric CFC-11, CFC-12, and N_2O abundances. Geophysical Research Letters, 48, e2021GL093700. https://doi. org/10.1029/2021GL093700, 2021.
Lovenduski, N.S., Gruber, N., Doney, S.C., and Lima, I.D.: Enhanced CO_2 outgassing in the Southern Ocean from a positive phase of the Southern Annular Mode, Glob. Biogeochem. Cycles 21, GB2026, doi:10.1029/2006GB002900, 2007.
Lueker, T.J., Walker, S.J., Vollmer, M.K., Keeling, R.F., Nevison, C.D. and Weiss, R.F.: Coastal upwelling air-sea fluxes revealed in atmospheric observations of O_2/N_2, CO_2 and N_2O, Geophys. Res. Lett., 30, 1292, 2003.
MacFarling Meure, C., Etheridge, D. M., Trudinger, C. M., Steele, L. P., Langenfelds, R. L., van Ommen, T., Smith, A. and Elkins, J. W.: Law Dome CO_2, CH_4, and N_2O ice core records extended to 2000 years BP, Geophys. Res. Lett., 33, L14810, doi:10.1029/2006GL026152, 2006.
Mahowald, N. M., Rasch, P. J., Eaton, B. E., Whittlestone, S. and Prinn, R. G.: Transport of radon-222 to the remote troposphere using the Model of Atmospheric Transport and Chemistry and assimilated winds from ECMWF and the National Center for Environmental Prediction/NCAR, J. Geophys. Res., 102, 28139–28151, 1997.
Masarie, K. A. and Tans, P.P.: Extension and integration of atmospheric carbon dioxide data into a globally consistent measurement record, Journal of Geophysical Research-Atmospheres, 100, D6, 11593-11610, 1995.
McPhaden, M. J., et al.: The tropical ocean-global atmosphere observing system: A decade of progress, J. Geophys. Res., 103, 14,169–14,240, doi:10.1029/97JC02906, 1998.
Minganti, D., Chabrillat, S., Christophe, Y., Errera, Q., Abalos, M., Prignon, M., Kinnison, D. E., and Mahieu, E.: Climatological impact of the Brewer–Dobson circulation on the N2O budget in WACCM, a chemical reanalysis and a CTM driven by four dynamical reanalyses, Atmos. Chem. Phys., 20, 12609– 12631, https://doi.org/10.5194/acp-20-12609-2020, 2020.
Minganti, D., Chabrillat, S., Errera, Q., Prignon, M., Kinnison, D. E., Garcia, R. R., et al. (2022). Evaluation of the N2O rate of change to understand the stratospheric Brewer-Dobson circulation in a Chemistry-Climate Model. Journal of Geophysical Research: Atmospheres, 127, e2021JD036390. https://doi.org/10.1029/2021JD036390.
Mosier, A.R., Duxbury, J.M., Freney, J.R., Heinemeyer, O. and Minami, K.: Assessing and mitigating N_2O emissions from agricultural soils, Climatic Change, 40, 7-38, 2000.

Naqvi, S.W.A., Jayakumar, D.A., Narvekar, P.V., Naik, H., Sarma, V.V.S.S., D'Sousa, W., Joseph, S., and George, M.D.: Increased marine production of N_2O due to intensifying anoxia on the Indian continental shelf, Nature, 408, 346-349, 2000.

Nash, E.R., Newman, P.A., Rosenfield, J.E., and Schoeberl, M.R.: An objective determination of the polar vortex using Ertel's potential vorticity, J. Geophys. Res., 101, 9471-9478, 1996.

National Oceanic Atmospheric Administration (NOAA) Global Monitoring Division, Interactive Data Visualization, https://www.esrl.noaa.gov/gmd/dv/iadv/, accessed April 6, 2021.

Nevison, C.D., Weiss, R.F. and Erickson III, D.J.: Global Oceanic Nitrous Oxide Emissions, J. Geophys. Res., 100, 15,809-15,820, 1995.

Nevison, C.D., Kinnison, D.E. and Weiss, R.F.: Stratospheric Influence on the tropospheric seasonal cycles of nitrous oxide and chlorofluorocarbons, Geophys. Res. Lett. 31(20), L20103, doi:10.1029/2004GL020398, 2004.

Nevison, C.D., Keeling, R.F., Weiss, R.F., Popp, B.N., Jin, X., Fraser, P.J, Porter, L.W. and Hess, P.G.: Southern Ocean ventilation inferred from seasonal cycles of atmospheric N_2O and O_2/N_2 at Cape Grim, Tasmania, Tellus, 57B, 218-229, 2005.

Nevison, C. D., Mahowald, N. M., Weiss, R.F. and Prinn, R.G.: Interannual and seasonal variability in atmospheric N_2O, Global Biogeochem. Cy., 21, GB3017, doi:10.1029/2006GB002755, 2007.

Nevison, C.D., Dlugokencky, E., Dutton, G., Elkins, J.W., Fraser, P., Hall, B., Krummel, P.B., Langenfelds, R.L., O'Doherty, S., Prinn, R.G., Steele, L.P., Weiss, R.F.: Exploring causes of interannual variability in the seasonal cycles of tropospheric nitrous oxide, Atmospheric Chemistry and Physics, 11, doi:10.5194/acp-11-1-2011, 1-18, 2011.

Nevison, C., Andrews, A., Thoning, K., Dlugokencky, E., Sweeney, C., Miller, S., et al.: Nitrous oxide emissions estimated with the CarbonTracker-Lagrange North American regional inversion framework. Global Biogeochemical Cycles, 32. https://doi. org/10.1002/2017GB005759, 2018.

Newman, P.: The Quasi-biennial Oscillation (QBO). Retrieved from https://acd-ext.gsfc.nasa.gov/Data_services/met/qbo/qbo.html, 2020.

Nielsen, J.E., Pawson, S., Molod, A., Auer, B., da Silva, A.M., Douglass, A.R., et al.: Chemical mechanisms and their applications in the Goddard Earth Observing System (GEOS) Earth system model, Journal of Advances in Modeling Earth Systems, 9(8), 3019-3044, doi:10.1002/2017MS001011, 2017.

Olivier, J.G.J., Van Aardenne, J.A., Dentener, F., Ganzeveld, L. and Peters, W.: Recent trends in global greenhouse gas emissions: regional trends and spatial distribution of key sources. In: Non-CO_2 Greenhouse Gases (NCGG-4), van Amstel, A. (coord.), page 325-330. Millpress, Rotterdam, 2005.

Park, S., et al.: Trends and seasonal cycles in the isotopic composition of nitrous oxide since 1940, Nature Geoscience, 5, 261-265, 2012.

Plumb, R. A.: Stratospheric transport, J. Meteorol. Soc. Jpn., 80, 793–809, 2002.

Prather, M. Hsu, J., J., DeLuca, N.M., Jackman, C.H., Oman, L.D., Douglass, A.R., Fleming, E.L., Strahan, S.E., Steenrod, S.D., Sovde, O.A., Isaksen, I.S.A., Froidevaux, L., Funke, B.: Measuring and modeling the lifetime of nitrous oxide including its variability, J. Geophys. Res. Atmos., 120, doi:10.1002/2015JD023267, 2015.

Prinn, R.G., Weiss, R.F., Fraser, P.J., Simmonds, P.G., Cunnold, D.M., Alyea, F.N., O'Doherty, S., Salameh, P., Miller, B.R., Huang, J., Wang, R.H.J., Hartley, D.E., Harth, C., Steele, L.P., Sturrock, G.,

Midgley, P.M. and McCulloch, A.: A history of chemically and radiatively important gases in air deduced from ALE/GAGE/AGAGE, J. Geophy. Res., 105 (D14), 17751-17792, 2000.

Ravishankara A. R., Daniel, J. S. and Portmann, R. W.: Nitrous Oxide (N_2O): The dominant ozone depleting substance emitted in the 21st century, Science, 326,123-125, doi: 10.1126/science.1176985, 2009.

Ray, E. A., Portmann, R. W., Yu, P., Daniel, J., Montzka, S. A., Dutton, G. S., et al.: The influence of the stratospheric Quasi-Biennial Oscillation on trace gas levels at the Earth's surface. Nature Geoscience, 13(1), 22–27. https://doi.org/10.1038/s41561-019-0507-3, 2020.

Ruiz, D.J., Prather, M.J., Strahan, S.E., Thompson, R.L., Froidevaux, L., and Steenrod, S.D.: How atmospheric chemistry and transport drive surface variability of N_2O and CFC-11, J. Geophys. Res., 2021.

Santoni, G. W., Daube, B. C., Kort, E. A., Jiménez, R., Park, S., Pittman, J. V., Gottlieb, E., Xiang, B., Zahniser, M. S., Nelson, D. D., McManus, J. B., Peischl, J., Ryerson, T. B., Holloway, J. S., Andrews, A. E., Sweeney, C., Hall, B., Hintsa, E. J., Moore, F. L., Elkins, J. W., Hurst, D. F., Stephens, B. B., Bent, J., and Wofsy, S. C.: Evaluation of the airborne quantum cascade laser spectrometer (QCLS) measurements of the carbon and greenhouse gas suite – CO_2, CH_4, N_2O, and CO – during the CalNex and HIPPO campaigns, Atmos. Meas. Tech., 7, 1509–1526, https://doi.org/10.5194/amt-7-1509-2014, 2014.

Sokal, R.R. and Rohlf, F.J.: Biometry, 859 pp., W.H. Freeman, New York, 1981.

Scaife, A.A. and James, I.N. (2000), Response of the stratosphere to interannual variability of tropospheric planetary waves. Q.J.R. Meteorol. Soc., 126: 275- 297. https://doi.org/10.1002/qj.49712656214.

Stephens, B.: ORCAS Merge Products. Version 1.0, https://doi.org/10.5065/D6SB445X, accessed 13 Jul 2020, 2017.

Stephens, B. B., Long, M. C., Keeling, R. F., Kort, E. A., Sweeney, C., Apel, E. C., Atlas, E. L., Beaton, S., Bent, J. D., Blake, N. J., Bresch, J. F., Casey, J., Daube, B. C., Diao, M., Diaz, E., Dierssen, H., Donets, V., Gao, B.-C., Gierach, M., Green, R., Haag, J., Hayman, M., Hills, A. J., Hoecker-Martínez, M. S., Honomichl, S. B., Hornbrook, R. S., Jensen, J. B., Li, R.-R., McCubbin, I., McKain, K., Morgan, E. J., Nolte, S., Powers, J. G., Rainwater, B., Randolph, K., Reeves, M., Schauffler, S. M., Smith, K., Smith, M., Stith, J., Stossmeister, G., Toohey, D. W., and Watt, A. S.: The O2/N2 Ratio and CO2 Airborne Southern Ocean Study, B. Am. Meteorol. Soc., 99, 381–402, https://doi.org/10.1175/BAMS-D-16-0206.1, 2018.

Shepherd, T. G.: Transport in the middle atmosphere, J. Meteorol. Soc. Jpn. Ser. II, 85, 165–191, 2007. Tian, H., Xu, R., Canadell, J.G. et al. A comprehensive quantification of global nitrous oxide sources and sinks. Nature 586, 248\u2013256 (2020). https://doi.org/10.1038/s41586-020-2780-0.

Stohl, A.: A 1-year Lagrangian "climatology" of airstreams in the Northern Hemisphere tropo- sphere and lowermost stratosphere, J. Geophys. Res., 106(D7), 7263–7279, 2001.

Strahan, S. E., Oman, L.D., Douglass, A.R. and Coy, L.: Modulation of Antarctic vortex composition by the quasi-biennial oscillation, Geophys. Res. Lett., 42, 4216–4223, doi:10.1002/2015GL063759, 2015.

Thompson, R.L., Dlugokencky, E., Chevallier, F., Ciais, P., Dutton, G., Langenfelds, R.L., Prinn, R.G.,

Weiss, R.F., Tohjima, Y., O'Doherty, S., Krummel, P.B., Fraser, P., and Steele, L.P.: Interannual variability in tropospheric nitrous oxide, 2013, Geophys. Res. Lett., 40, 4426-4431, doi:10.1002/grl.50721, 2013.

Thompson, R. L., Patra, P. K., Ishijima, K., Saikawa, E., Corazza, M., Karstens, U., et al.: TransCom N2O model inter-comparison-Part 1: Assessing the influence of transport and surface fluxes on tropospheric N2O variability, Atmospheric Chemistry and Physics, 14(8), 4349–4368. https://doi.org/10.5194/acp-14-4349-2014a.

Thompson, R. L., Ishijima, K., Saikawa, E., Corazza, M., Karstens, U., Patra, P. K., Bergamaschi, P., Chevallier, F., Dlugokencky, E., Prinn, R. G., Weiss, R. F., O'Doherty, S., Fraser, P. J., Steele, L. P., Krummel, P. B., Vermeulen, A., Tohjima, Y., Jordan, A., Haszpra, L., Steinbacher, M., Van der Laan, S., Aalto, T., Mein- hardt, F., Popa, M. E., Moncrieff, J., and P. Bousquet: TransCom N_2O model inter-comparison, Part II: Atmospheric inversion es- timates of N_2O emissions, Atmos. Chem. Phys. Discuss., 14, 5271–5321, doi:10.5194/acpd-14-5271-2014, 2014b.

Thompson, R.L., Lassaletta, L., Patra, P.K., Wilson, C., Wells, K.C., Gressent, A., Koffi, E.N., Chipperfield, M.P., Winiwarter, W., Davidson, E.A., Tian, H. and Canadell, J.G.: Acceleration of global N_2O emissions seen from two decades of atmospheric inversion, Nature Climate Change, https://doi.org/10.1038/s41558-019-0613-7, 2019.

Thompson, T.M., Elkins, J.W., Hall, B., Dutton, G.S., Swanson, T.H., Butler, J.H., Cummings, S.O., Fisher, D.A.: Halocarbons and other Atmospheric Trace Species, in: Schnell, R.C., A.-M. Buggle and R.M. Rossson (Eds.), Climate Diagnostics Laboratory Summary Report #27, 2002-2003, US Department of Commerce, National Oceanic and Atmospheric Administration, Boulder, Colorado, 2004.

Thompson, C.R., Wofsy, S.C., Prather, M.J., Newman, P.A., Hanisco, T.F., Ryerson, T.B., Fahey, D.W., Apel, E.C., Brock, C.A., Brune, W.H. et al.: The NASA Atmospheric Tomography (ATom) mission: Imaging the chemistry of the global atmosphere, Bulletin of the American Meteorological Society, 103 (3): E761–E790. DOI: http://dx.doi.org/10.1175/bams-d-20-0315.1, 2022.

Tian, H., Xu, R., Canadell, J.G., Thompson, R.L., Winiwarter, W., Suntharalingam, P., Davidson, E.A., Ciais, P., et al.: A comprehensive quantification of global nitrous oxide sources and sinks, Nature, 586, 248-255. https://doi.org/10.1038/s41586-020-2780-0, 2020.

Volk, C.M., Elkins, J.W., Fahey, D., Dutton, G., Gilligan, J., Lowenstein, M., Podolske, J., Chan, K., and Gunson, M.: Evaluation of source gas lifetimes from stratospheric observations, J. Geophys. Res., 102(D21), 25,543-25,564, 1997.

Waugh, D.W., Randel, W.J., Pawson, S., Newman, P.A. and Nash, E.R.: Persistence of the lower stratospheric polar vortices, J. Geophys. Res., 104 (D22), 27,191-27,201, 1999.

Weiss, R.F.: The temporal and spatial distribution of tropospheric nitrous oxide, J. Geophys. Res. 86, 7185-7195, 1981.

Wofsy, S. C., the HIPPO Science Team and Cooperating Modellers and Satellite Teams: HIAPER Pole-to-Pole Observations (HIPPO): Fine grained, global scale measurements for determining rates for transport, surface emissions, and removal of climatically important atmospheric gases and aerosols, Phil. Trans. of the Royal Society A, 369(1943), doi:10.1098/rsta.2010.0313, 2073-2086, 2011.

Wofsy, S., Afshar, S., Allen, H., Apel, E., Asher, E., Barletta, B., Bent, J., Bian, H., Biggs, B., Blake, D., and et al.: ATom: Merged Atmospheric Chemistry, Trace Gases, and Aerosols, https://doi.org/10.3334/ORNLDAAC/1581, accessed 13 Jul 2020, 2018.

Wofsy, S., Daube, B., Jimenez, R., Kort, E., Pittman, J., Park, S., Commane, R., Xiang, B., Santoni, G., Jacob, D., and et al.: HIPPO Merged 10-Second Meteorology, Atmospheric Chemistry, and Aerosol Data. Version 1.0, https://doi.org/10.3334/CDIAC/HIPPO_010, accessed 13 Jul 2020, 2017.

WMO Greenhouse Gas Bulletin No. 14, https://library.wmo.int/ doc_num.php?explnum_id=5455, 2018.

Yang, S. et al.: Global reconstruction reduces the uncertainty of oceanic nitrous oxide emissions and reveals a vigorous seasonal cycle, Proceedings of the National Academy of Sciences, 117(22), 11954–11960, doi:10.1073/pnas.1921914117, 2020.